Journal of Medicinal Chemistry

Article

Small Molecule Inhibitors Simultaneously Targeting Cancer Metabolism and Epigenetics: Discovery of Novel Nicotinamide Phosphoribosyltransferase (NAMPT) and Histone Deacetylase (HDAC) Dual Inhibitors

Guoqiang Dong, Wei Chen, Xia Wang, Xinglin Yang, Tianying Xu, Pei Wang, Wannian Zhang, Yu Rao, Chao-Yu Miao, and Chunquan Sheng

J. Med. Chem., **Just Accepted Manuscript** • DOI: 10.1021/acs.jmedchem.7b00467 • Publication Date (Web): 08 Sep 2017

ACS Publications

Journal of Medicinal Chemistry is published by the American Chemical Society. 1155 Sixteenth Street N.W., Washington, DC 20036

Small Molecule Inhibitors Simultaneously Targeting Cancer Metabolism and Epigenetics: Discovery of Novel Nicotinamide Phosphoribosyltransferase (NAMPT) and Histone Deacetylase (HDAC) Dual Inhibitors

Guoqiang Dong[†,1], Wei Chen[†,1], Xia Wang[†,1], Xinglin Yang[2], Tianying Xu[1], Pei Wang[1], Wannian Zhang[1], Yu Rao*[,2], Chaoyu Miao*[,1], Chunquan Sheng*[,1]

[1] *School of Pharmacy, Second Military Medical University, 325 Guohe Road, Shanghai 200433, People's Republic of China*

[2] *MOE Key Laboratory of Protein Sciences, School of Pharmaceutical Sciences, Tsinghua University, Beijing 100084, People's Republic of China*

ABSTRACT

Cancer metabolism and epigenetics are among the most intensely pursued research areas in anticancer drug discovery. Here we report the first small molecules that simultaneously inhibit nicotinamide phosphoribosyltransferase (NAMPT) and histone deacetylase (HDAC), two important targets of cancer metabolism and epigenetics, respectively. Through iterative structure-based drug design, chemical synthesis and biological assays, a highly potent dual NAMPT and HDAC inhibitor was successfully identified. Compound **35** possessed excellent and balanced activities against both NAMPT (IC_{50} = 31 nM) and HDAC1 (IC_{50} = 55 nM). It could effectively induce cell apoptosis and autophagy and ultimately led to cell death. Importantly, compound **35** showed excellent *in vivo* antitumor efficacy in the HCT116 xenograft model. This proof-of-concept study demonstrates the feasibility of discovering an inhibitor targeting cancer metabolism and epigenetics and provides an efficient strategy for multi-target antitumor drug discovery.

Keywords: NAMPT, HDAC, dual inhibitor, structure-based design, antitumor activity.

INTRODUCTION

In recent decades, drug discovery has been strongly focused on the development of drugs acting against a specific biological target with high potency and selectivity.[1, 2] This paradigm is based on the lock and key model proposed by Fischer and has led to numerous successful drugs in the market.[3] However, single target drugs might not achieve the desired therapeutic effects for the treatment of complex diseases such as cancer. The underlying reason is that the dysregulation of multiple signaling pathways is a hallmark of cancer development and progression, and the existence of compensating signaling pathways has reduced the efficacy of single target drugs.[4-6] Specific drug combinations have expanded the treatment to achieve more durable disease control. However, the employment of drug cocktails often complicates the doses/schedule and negatively impacts patient compliance. It can also introduce the unpredictable pharmacokinetic (PK) profile and drug-drug interactions.[2] In contrast, a single multi-target molecule has the advantages of higher synergistic effect, more predictable PK profile, reduced compliance difficulties and so on.[1] However, rational design of multi-target drugs still remains a highly challenging task, particularly for the targets belong to different protein families. The difficulties mainly include the identification of the most suited combination of targets, achieving the balanced or desired activities against different targets, complex optimization of polypharmacology profile and drug-likeness to transform leads into drug candidates.[1, 2, 7] For example, with deep understanding of tumor pathogenesis, multi-target antitumor agents have been considered as an important strategy to overcome drug resistance and improve

therapeutic effects.[1, 2, 4, 8]

Epigenetic regulation has played an important role in the onset and progression of human diseases.[9] Specifically, histone deacetylases (HDACs) are a family of epigenetic enzymes that has achieved great success for cancer therapeutics.[9] HDAC inhibitors (HDACi) have been recently developed as potent antineoplastic agents. Four of them, **1** (SAHA, **Figure 1A**), FK228, PXD-101 and LBH-589 have been approved by FDA for the treatment of hematologic cancer.[10-13] However, treatment of solid tumors by HDACi still remains a big challenge and discovery of HDACi-based multi-target antitumor agents may be an effective strategy.[14, 15]

Cancer is a disease of genetic heterogeneity, but the metabolic alteration is the common feature of malignant cells.[16, 17] During the past decade, targeting cancer metabolism has emerged as a promising strategy for the development of antitumor agents.[18] Among these targets, nicotinamide adenine dinucleotide (NAD) metabolism has attracted broad interests because of its essential role in a number of cellular process to sustain tumor cell growth and survival.[19] NAD is an important cofactor that plays a central role in cellular redox reactions and serves as a second messenger for a number of cellular process for survival. In mammalian cells, there are three main pathways for NAD biosynthesis (**Figure S1** in supporting information): a *de novo* pathway synthesized from tryptophan (Trp), the primary salvage pathway using nicotinamide (NAM) as the precursor, and the alternative salvage pathway dependent on nicotinic acid.[17, 20] In humans, the main source of cellular NAD is from primary salvage pathway using NAM, and nicotinamide phosphoribosyltransferase (NAMPT)

is the rate-limiting enzyme. Cancer cells have an increased demand for ATP and consume NAD at a higher rate than normal tissues. Inhibition of NAMPT can dramatically impact NAD metabolism and cancer proliferation. Thus, NAMPT has emerged as an attractive target for the development of anticancer therapeutics.[17, 21] To date, a number of novel and potent NAMPT inhibitors have been reported.[17, 20, 22] Among them, **2** (FK866, **Figure 1B**) and **3** (CHS828) have been progressed to human clinical trials.[23-25] However, their clinical development of has been hampered by toxicity such as dose-limiting thrombocytopenia.[26, 27]

NAMPT inhibitor **2** was proven to synergistically enhance the inhibitory effect of HDACi,[28] suggesting that dual NAMPT/HDAC inhibitors are likely to possess promising antitumor profiles (**Table S1** in Supporting Information). Moreover, the structural features and pharmacophore of NAMPT and HDAC inhibitors (**Figure 1**) offer an opportunity to design dual NAMPT/HDAC inhibitors. Herein, the first dual NAMPT/HDAC inhibitors were rationally designed, synthesized and assayed. Interestingly, a highly potent inhibitor with balanced activity against NAMPT/HDAC and excellent *in vivo* antitumor potency was successfully identified.

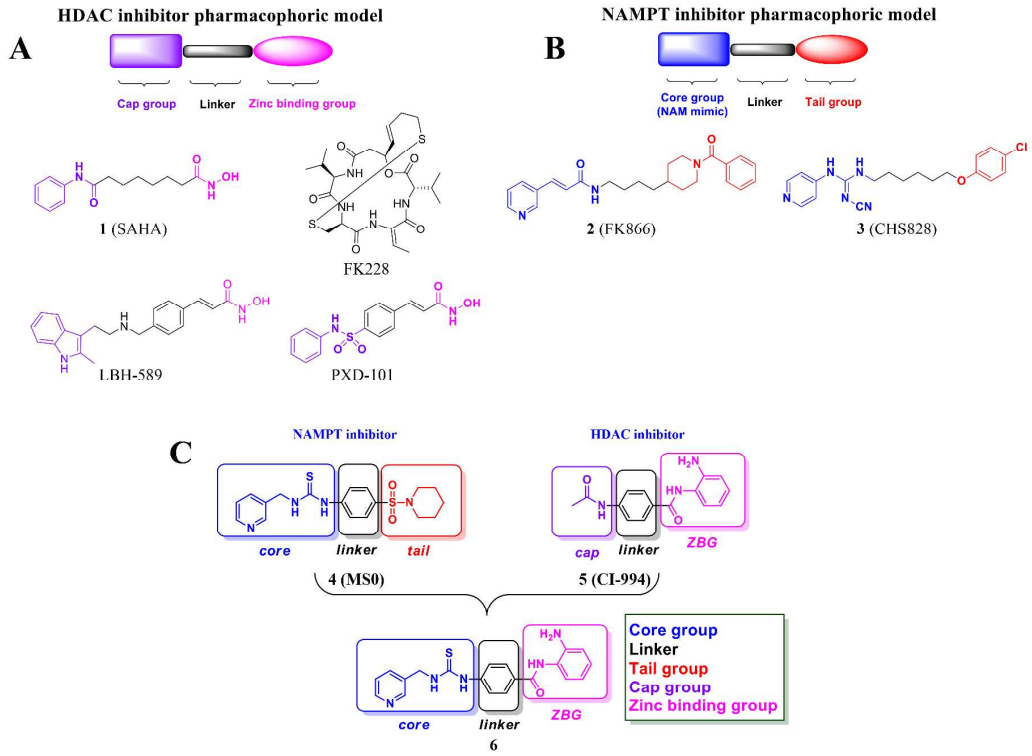

Figure 1. Pharmacophoric model and chemical structures of the NAMPT (**A**) and HDAC (**B**) inhibitors. (**C**) Identification of **6** as a NAMPT/HDAC dual inhibitor.

RESULTS AND DISCUSSION

Chemistry. The synthetic routes of the target compounds are shown in **Schemes 1-5**. Compounds **12a-t** were prepared by the procedure detailed in **Scheme 1**. Reduction of commercially available starting material **7** with Raney Ni and H_2 led to intermediate **8**. 4-Aminobenzoic acid was treated with 1,1'-thiocarbonyldiimidazole (TCDI) or *N*,*N*'-carbonyldiimidazole (CDI) to give isothiocyanate or isocyanate **10**, which was condensed with intermediate **8** to yield thioureas or ureas (**11a-t**). Condensation of compound **11a-t** with *o*-phenylenediamine afforded the target compounds **12a-t**.

Scheme 1

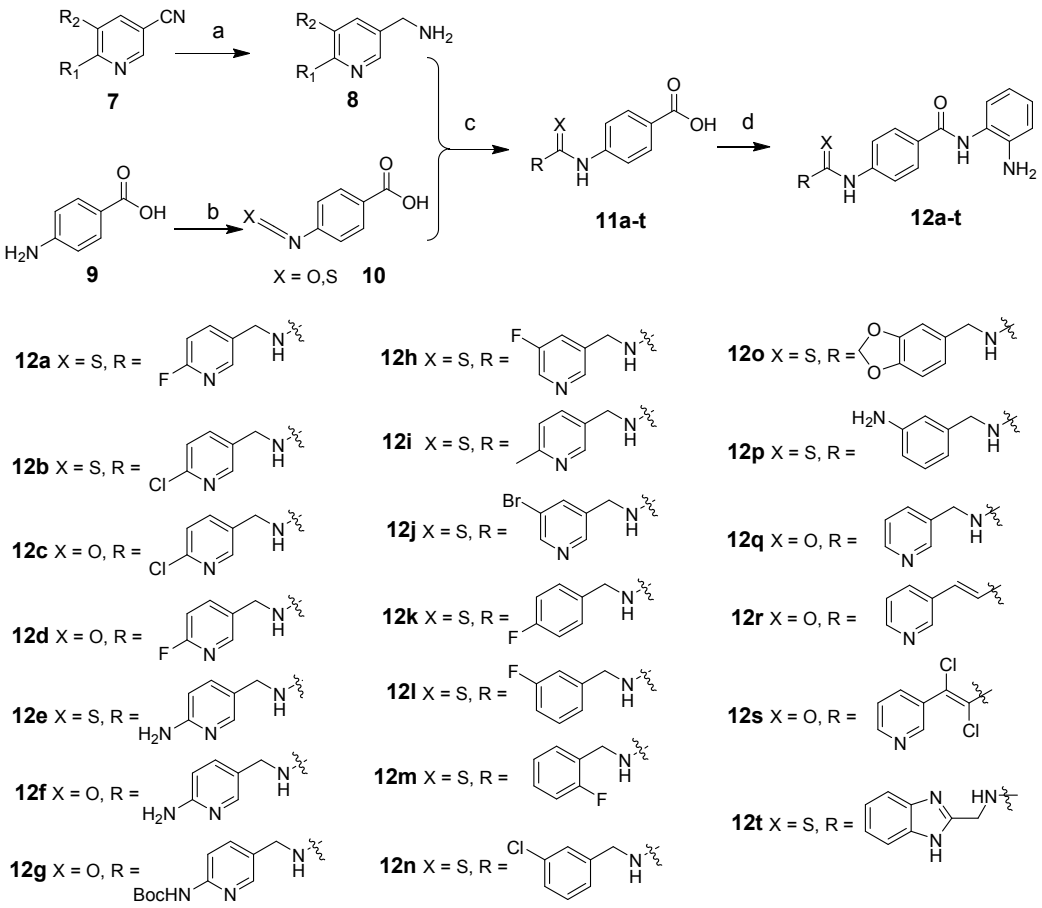

Reagents and conditions: (a) Raney Ni, H_2, NH_3/MeOH, rt, 12 h, yield 21-89%; (b) CDI or TCDI, CH_2Cl_2, rt, 2 h, yield 85-95%; (c) THF, rt, 12 h, yield 62-81%; (d) *o*-phenylenediamine, HBTU, Et_3N, DMF, rt, 3 h, yield 43-75%.

Replacement of core group with various binary heterocycle-derived amides and introducing a methylene between the amide and phenyl linker moiety gave compounds **16a-g** (**Scheme 2**). Methyl 4-(aminomethyl) benzoate was condensed with carboxylic acids to provide intermediates **14a-g**. Then, treatment of compounds **14a-g** with LiOH followed by coupling with *o*-phenylenediamine gave target compounds **16a-g**.

Scheme 2

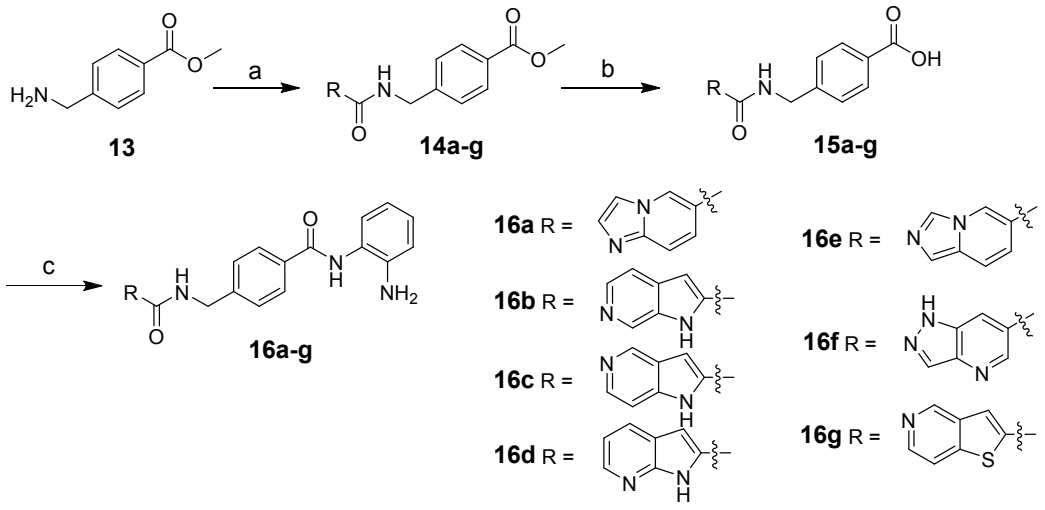

Reagents and conditions: (a) R-COOH, EDC, DMAP, DMF, rt, 3 h, yield 31-69%; (b) LiOH, THF/MeOH/H_2O, rt, 24 h, yield 82-97%; (c) *o*-phenylenediamine, HBTU, Et_3N, DMF, rt, 4 h, yield 37-75%.

Compounds **24** was synthesized according to the procedures outlined in **Scheme 3**. Starting from 3-iodopyridine (**17**), intermediate **19** was prepared *via* two steps according to the reported methods.[29] Methyl 4-(2-bromoethyl)benzoate was reacted with NaN_3 to give azide **21**, which was coupled with intermediate **19** by copper(I)-catalyzed click reaction at room temperature to obtain 1,4-disubstituted 1,2,3-triazole **22**.[30] Hydrolysis of the methylester in **22** gave the acid **23**, which were condensed with *o*-phenylenediamine to afford target compound **24**.

Scheme 3

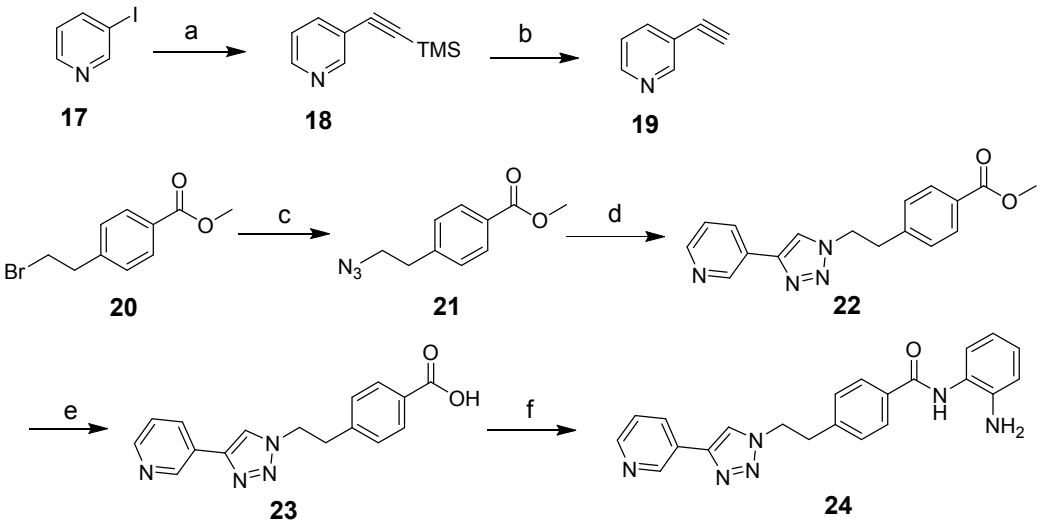

Reagents and conditions: (a) Ethynyltrimethylsilane, $Pd_2(PPh_3)_2$, CuI, Et_3N, rt, 1 h; (b) K_2CO_3, MeOH, rt, 0.5 h, yield 81% over two steps; (c) NaN_3, DMF, 80 ^oC, 8 h, yield 85%; (d) **19**, $CuSO_4 \cdot 5H_2O$, VcNa, N_2, *t*-butanol/H_2O, rt, 12 h, yield 82%; (e) LiOH, THF/MeOH/H_2O, rt, 24 h, yield 90%; (f) *o*-phenylenediamine, HBTU, Et_3N, DMF, rt, 4 h, yield 27%.

As shown in **Scheme 4**, 4-ethynylaniline (**25**) was reacted with CDI to produce isocyanate **26**, which was treated with 3-(aminomethyl)pyridine to give intermediate **27**. Compound **28** was obtained by click reaction of methyl 4-(azidomethyl)benzoate with **27**. Hydrolysis of **28** gave the acid **29**, which were condensed with *o*-phenylenediamine to afford target compounds **30**. Compound **35** was synthesized according the procedure described in **Scheme 5**. Condensation of 4-ethynylbenzoic acid (**31**) with 3-(aminomethyl)pyridine in the present of HBTU (*o*-benzotriazole-*N*,*N*,*N*,*N*-tetramethyl-uronium -hexafluorophosphate) and Et_3N gave

intermediate **32**. Finally, compounds **35** was prepared using the condition similar to that of compounds **30**.

Scheme 4

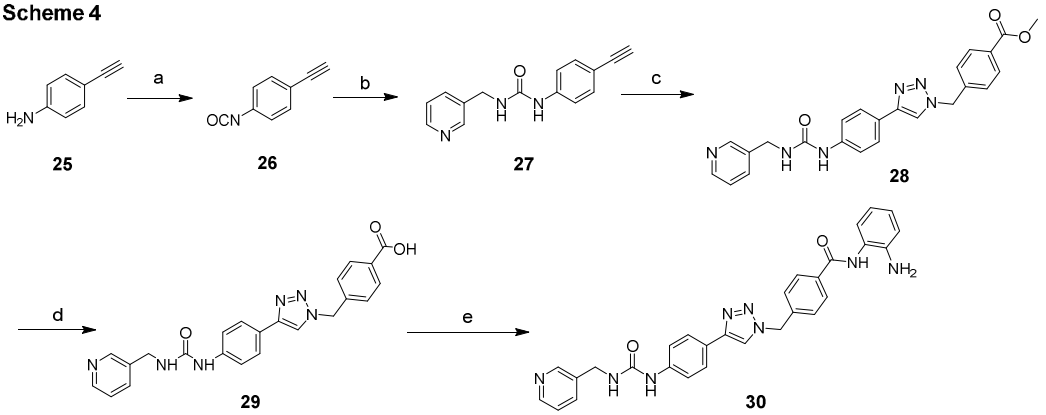

Reagents and conditions: (a) CDI, THF, rt, 2 h; (b) 3-(aminomethyl)pyridine, THF, rt, 12 h, yield 74% over two steps; (c) methyl 4-(azidomethyl)benzoate, $CuSO_4 \cdot 5H_2O$, VcNa, N_2, *t*-butanol/H_2O, rt, 12 h, yield 69%; (d) LiOH, THF/MeOH/H_2O, rt, 24 h, yield 93%; (e) HBTU, Et_3N, DMF, rt, 3 h, yield 68%.

Scheme 5

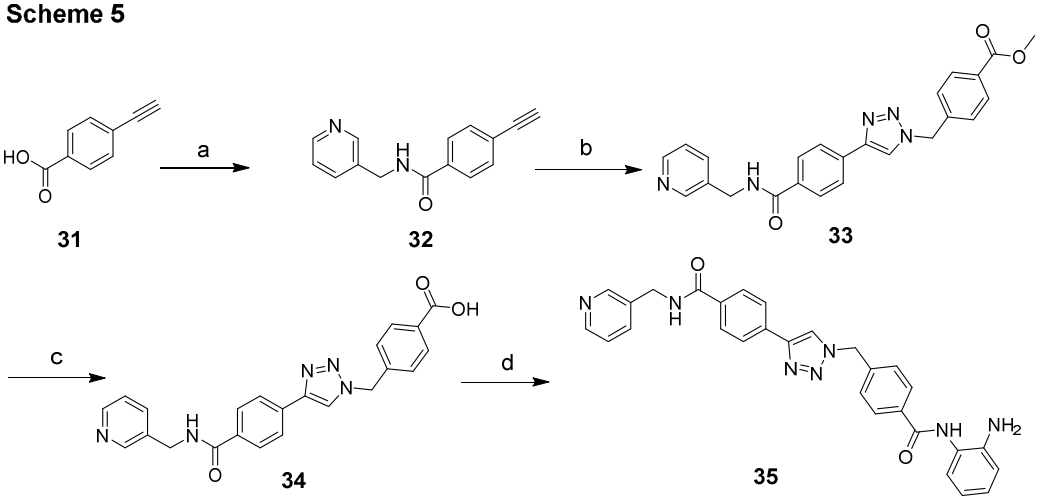

Reagents and conditions: (a) 3-(aminomethyl)pyridine, HBTU, Et_3N, DMF, rt, 3 h, yield 45%; (b) methyl 4-(azidomethyl)benzoate, $CuSO_4 \cdot 5H_2O$, VcNa, N_2, *t*-butanol/H_2O, rt, 12 h, yield 67%; (c) LiOH, THF/MeOH/H_2O, rt, 24 h, yield 81%;

(d) *o*-phenylenediamine, HBTU, Et_3N, DMF, rt, 3 h, yield 50%.

Structure-based Design of Novel NAMPT/HDAC Dual Inhibitors. Generally, NAMPT inhibitors are linear in shape and the pharmacophore consists of a core (or cap) group as the NAM mimetic (typically a meta or para substituted pyridine), a linker and a relatively narrow and hydrophobic tail group (**Figure 1C**).[20] Previously, our group identified a series of novel NAMPT inhibitors by high throughput screening and structure-based design.[22, 31, 32] Among them, compound **4** (MS0) is a highly active inhibitor containing typical pharmacophoric groups, namely a core binding moiety (pyridinylmethylthiourea), a linker (phenyl group) and a tail group (piperidinesulfonyl group).[22, 33] Interestingly, HDAC inhibitors share similar molecular shape and structural characteristics to those of NAMPT inhibitors (**Figure 1C**). Briefly, typical HDAC inhibitors contain a zinc-binding group (ZBG, hydroxamic acid or *ortho*-aminoanilide), a linker and a hydrophobic cap group.[34] Based on the structural features of **4**, we envisioned that NAMPT/HDAC dual inhibitors could be designed by fusion of the pharmacophore of **4** with HDAC inhibitor **5** (CI-994, **Figure 1C**).[35] To validate the hypothesis, a new compound (**6**) was designed by merging the core group (pyridinylmethylthiourea) of NAMPT inhibitor **4** with the ZBG motif (*N*-(2-aminophenyl)benzamide) in HDAC inhibitor **5** using a common phenyl linker.

Because current docking methods can accurately reproduce the binding modes of NAMPT and HDAC inhibitors (**Figure S2** in supporting information),[22, 36] compound **6** was subjected for molecular docking to investigate whether it can form favorite

interactions with the two targets. After the docking process, molecular dynamics simulations were performed on the docked complexes to further validate the stability and affinity of the obtained binding poses using Desmond/Maestro non-commercial version 2016.3 (**Figure S3** in supporting information).[37] As shown in **Figure 2A**, compound **6** interacted with NAMPT by a linear conformation. Its pyridinyl group formed face-to-face π-π interactions with Phe193 and Tyr18′, respectively. Two NH groups in thiourea formed hydrogen bonding interactions with the carboxyl group of Asp219. The terminal *N*-(2-aminophenyl)benzamide was located at the outside of active site. The terminal NH_2 group formed hydrogen bonding interaction with the backbone carbonyl group of Val350. For the binding mode of **6** with HDAC1, main interactions were involved in the linker and ZBG (**Figure 2B**). The phenyl linker and terminal phenyl group formed π-π stacking interaction with His141. Besides chelating with Zn^{2+}, the terminal *N*-(2-aminophenyl)benzamide group was engaged with a hydrogen bonding network with Gly149, His140 and Hisl41. The terminal NH_2 group formed two hydrogen bonds with the nitrogen atom in the imidazole of His140 and Hisl41, respectively. The amide NH group formed hydrogen bonding interaction with the backbone carbonyl group of Gly149. Based on the above analysis, compound **6** shares a similar binding mode with typical HDAC1 or NAMPT inhibitors. The sequence identity between human HDAC1 and HDAC2 is 86%.[38] Compound **6** was also docked into the HDAC2 (PDB: 3MAX) active pocket. The binding mode of compound **6** with HDAC2 was very similar to that with HDAC1 (detailed description provided in **Figure S4**, supporting information). Inspired by the modeling results,

compound **6** was synthesized (**Scheme S1** in Supporting Information) and assayed for inhibitory activity against NAMPT and HDAC1 using the method described before.[22, 39] In the NAMPT inhibitory assay, human recombinant NAMPT was used to catalyze NAM to NMN. The product NMM was quantified by reacting with acetophenone and formic acid, with the formation of fluorescent derivative detected with an excitation of 382 nm and an emission wavelength of 445 nm. In the HDAC1 inhibitory assays, substrate Ac-Leu-Gly-Lys(Ac)-AMC was deacetylated by recombinant HDAC1 and followed hydrolyzed by trypsin to release 7-amino-4-methylcoumarin (AMC). AMC was detected with an excitation of 350-360 nm and an emission wavelength of 450-460 nm. To our delight, compound **6** showed an IC_{50} value of 116 nM and 1.6 μM against NAMPT and HDAC1, respectively (**Figure 2C** and **2D**).

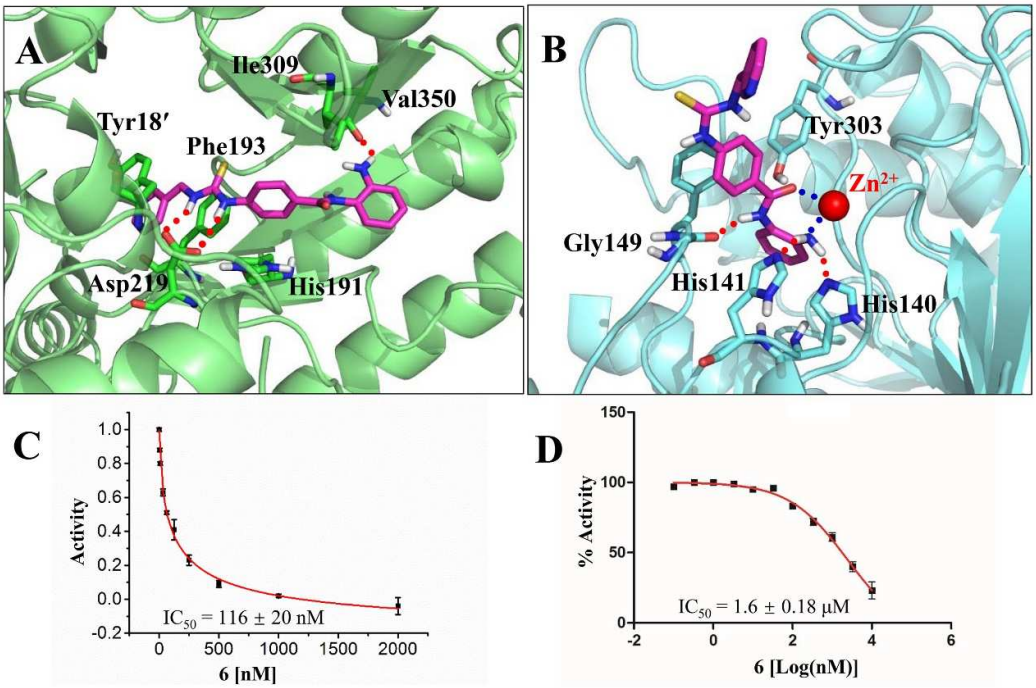

Figure 2. Identification of compound 6 as a NAMPT/HDAC dual inhibitor. (**A**) Proposed binding mode of compound **6** in the active site of NAMPT (PDB ID: 2GVJ). (**B**) Proposed binding mode of compound **6** in the active site of HDAC1 (PDB ID: 4BKX). The figure was generated using PyMol (http://www.pymol.org/). (**C**) Concentration response curve of **6** on NAMPT activity. (**D**) Concentration response curve of **6** on HDAC1 activity. Data are shown as mean ± standard deviation.

NAMPT/HDAC Dual Inhibitor 6 Exhibits Potent *In vitro* and *In vivo* Antitumor Activity. NAMPT/HDAC1 dual inhibitor **6** was further assayed for growth inhibitory activities toward human cancer cell-lines HCT116 (colon cancer) and HepG2 (liver cancer) using the MTT assay. Two lead compounds, NAMPT inhibitor **4** and HDAC inhibitor **5**, were used as reference drugs. As shown in **Figure 3A**, compound **6** showed good inhibitory activity against the HCT116 cell line (IC_{50} = 1.0 μM), which was more potent than **4** and **5**. Although the antitumor activity against HepG2 cell line was slightly decreased, compound **6** was still more active than the positive drugs. Therefore, compound **6** was progressed to *in vivo* mouse pharmacokinetic and xenograft efficacy studies. After single oral administration at a dose of 25 mg/kg, compound **6** demonstrated acceptable pharmacokinetic properties (**Figure S6** and **Table S2** in supporting information). The terminal half-life was approximately 1.8 h and the C_{max} was 2.3 μM. The *in vivo* antitumor potency of **6** was investigated in HCT116 xenograft nude mice models. After oral administration for 14 consecutive days, compound **6** achieved significant tumor growth inhibition (**Figure**

3B, $P < 0.05$) at the dose of 25 mg/kg/day. Moreover, it was observed to be well tolerated during the test and no significant loss of body weight was observed, indicating that its toxicity is low (**Figure 3C**).

A

Compound	Nampt (nM)	HDAC1 (μM)	HCT116 (μM)	HepG2 (μM)
6	116 ± 20	1.6 ± 0.18	1.0 ± 0.11	4.2 ± 0.37
4	9.9 ± 1.1	>10	41 ± 3.1	5.3 ± 0.45
5	>2000	1.2 ± 0.10	10 ± 2.3	10 ± 3.2

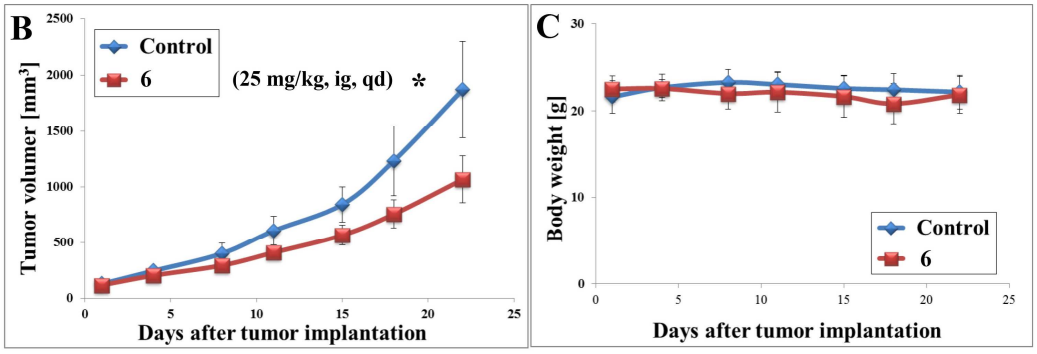

Figure 3. *In vitro* and *in vivo* antitumor efficacy of NAMPT/HDAC1 dual inhibitor **6**. (**A**) Enzyme inhibition and *in vitro* antitumor activity of compound **6**. (**B**) *In vivo* antitumor efficacy of compound **6** in the HCT116 tumor xenograft model. * $P < 0.05$, versus the control group, determined with Student's *t* test. (**C**) Body weight loss as a result of compound **6** administration in HCT116 xenograft experiment.

Structural Optimization and Structure-activity Relationship of NAMPT/HDAC Dual Inhibitor 6. Although compound **6** was proven to be a NAMPT/HDAC1 dual inhibitor and showed potent antitumor activity, its inhibitory activity against HDAC1 was only moderate and its antitumor activity remained to be further improved. Thus, further optimization studies were focused on achieving the balanced activity toward both targets and improving the *in vivo* antitumor potency. On

the basis of the binding mode of compound **6**, classical pharmacophore for NAMPT/HDAC dual inhibitors consists of a ZBG, a hydrophobic linker and a hydrophobic core group (**Figure 4**). *Ortho*-aminoanilide was chosen as the ZBG because it is one of the most wellknown group for chelating the zinc ion. Examination of the binding mode of **6** with NAMPT (**Figure 2A**) suggested that linking the *ortho*-aminoanilide as the tail group made the ZBG point to the solvent region and was well tolerable. The NAM mimetic (i.e. substituted pyridine) served as a core group, which intercalated at the site between Phe193 and Tyr18′ and formed π-π interactions. Because of the presence of large hydrophobic patches at the HDAC surface rim,[15] it was conceivable that the core group could form new interactions. Different linker moieties contained in reported potent NAMPT or HDAC inhibitors were analyzed and chosen as the hydrophobic linker group. Therefore, a series of derivatives were designed and synthesized by optimization of the core group and linker (**Figure 4**). Initially, the importance of pyridinyl core group was investigated by introducing substitutions (**12a-j**), pyridinyl/phenyl replacement (**12k-o**) and pyridine/heterocycle (**12t**, **16a-g**) replacement, which was supposed to form various interactions with NAMPT and HDAC. Then, the thiourea group was optimized by urea (**12q**) or α,β-unsaturated amide (**12r**, **12s**) to adjust the hydrogen bonding interaction. Finally, 1,2,3-triazole was introduced to achieve excellent and balanced dual inhibition (**24**, **30** and **35**) because the correponding binding pocket in NAMPT and HDAC could accomodate flexible linkers with different length. Most core and linker groups were selected from highly potent HDAC or NAMPT inhibitors, which

will be described in the following sections. Their *in vitro* data for inhibition of NAMPT/HDAC1 as well as the cytotoxicity toward HCT116 (colon cancer), HepG2 (liver cancer) and MDA-MB-231 (breast cancer) cells are listed in **Tables 1-2**. Compounds **1** and **2** were used as the reference drugs.

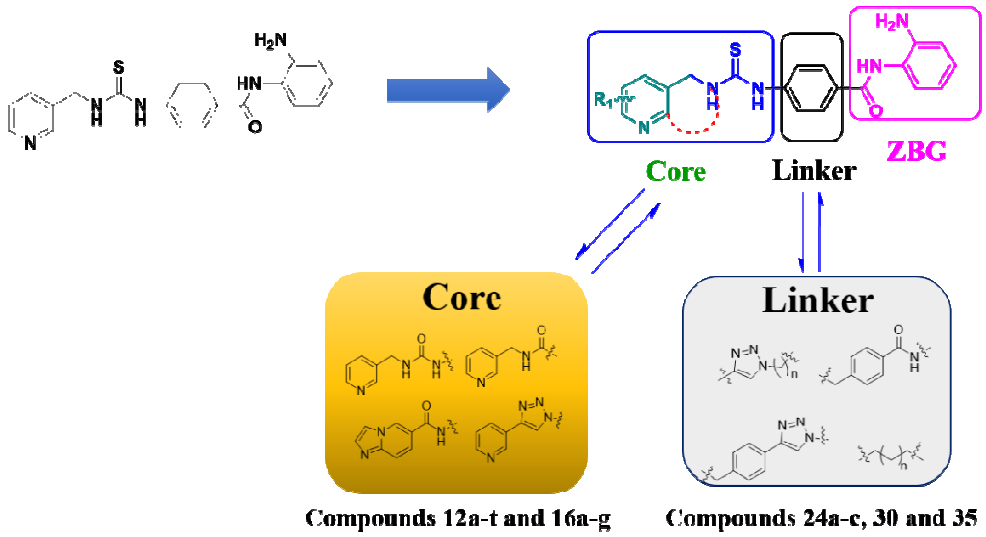

Figure 4. Design strategy of the NAMPT/HDAC1 dual inhibitors.

Initially, various substitutions were introduced on the pyridinyl group (compounds **12a-j**). These compounds generally showed improved inhibitory activity against HDAC1 (IC_{50} range: 0.021 μM - 0.37 μM). However, their inhibitory activities toward NAMPT were signicantly reduced (IC_{50} > 2 μM). Furthermore, the pyridinyl group was replaced by substituted phenyl groups (compounds **12k-p**) and nitrogen containing heterocycles[17, 33] (compounds **12t** and **16a-g**). Unfortunately, these derivatives did not show increased NAMPT inhibitory activity, although their good HDAC1 inhibitory activity was retained (**Table 1**).

To explain the SAR, compounds **12a** and **12k** were docked and superimposed with compound **6** in the active site of NAMPT (**Figure S5**). The binding mode of **12a** and **12k** was very similar to that of compound **6**. However, fluorine substituted pyridinyl and phenyl group could not act as the NAM mimetic because the fluorine atom occupied the position of pyrindine nitrogen atom of compound **6** (**Figure S5B**), which might be the reason why the NAMPT inhibitory activity of these compounds was decreased. Thus, it can be confirmed that the pyridine ring is essential for the NAMPT inhibitory activity.

Table 1. Enzyme inhibition and *in vitro* antitumor activity of the target compounds

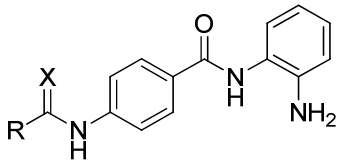

Compds	R	X	IC_{50} (μM)				
			NAMPT	HDAC1	HCT116	MDA-MB-231	HepG2
12a	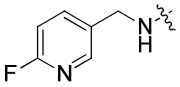	S	>2.0	0.37 ± 0.031	10 ± 2.6	81 ± 7.6	5.2 ± 0.55
12b	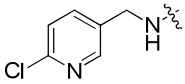	S	>2.0	0.25 ± 0.013	6.1 ± 0.51	42 ± 3.7	19 ± 2.7
12c	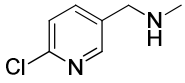	O	>2.0	0.021 ± 0.001	5.2 ± 0.47	34 ± 3.9	2.4 ± 0.19
12d	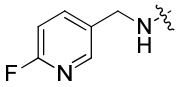	O	>2.0	0.28 ± 0.015	14.0 ± 1.7	91 ± 8.3	13 ± 0.10
12e	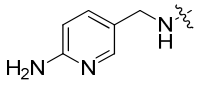	S	>2.0	0.20 ± 0.026	27 ± 2.3	>100	14 ± 1.5
12f	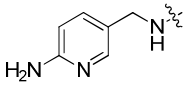	O	>2.0	0.33 ± 0.047	7.3 ± 0.80	>100	3.1 ± 0.28

12g	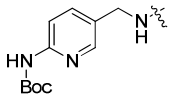	O	>2.0	3.3 ± 0.28	100 ± 12	>100	100 ± 9.3
12h	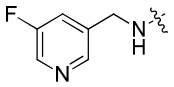	S	>2.0	0.44 ± 0.053	15 ± 1.9	85 ± 9.8	13 ± 1.2
12i	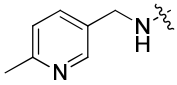	S	>2.0	0.26 ± 0.022	11 ± 2.1	63 ± 5.9	11 ± 2.1
12j	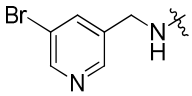	S	>2.0	0.35 ± 0.031	9.2 ± 0.79	39 ± 4.1	7.5 ± 0.63
12k	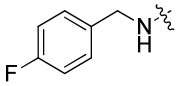	S	>2.0	0.30 ± 0.029	15 ± 1.9	>100	8.8 ± 7.5
12l	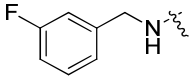	S	>2.0	0.17 ± 0.011	5.9 ± 0.62	74 ± 8.0	2.9 ± 0.22
12m	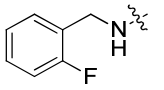	S	>2.0	0.30 ± 0.025	6.3 ± 0.54	>100	5.4 ± 0.56
12n	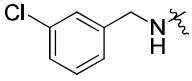	S	>2.0	0.18 ± 0.021	5.9 ± 0.49	92 ± 8.9	2.6 ± 0.23
12o	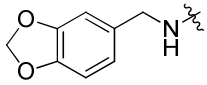	S	>2.0	0.10 ± 0.009	8.4 ± 0.77	>100	5.1 ± 0.49
12p	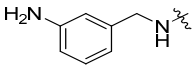	S	>2.0	0.22 ± 0.035	2.8 ± 0.19	>100	3.3 ± 0.30
12q	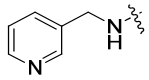	O	0.55 ± 0.047	0.22 ± 0.018	9.4 ± 0.88	>100	5.1 ± 0.48
12r	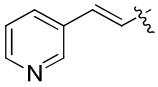	O	0.23 ± 0.029	0.62 ± 0.057	48 ± 5.0	>100	2.7 ± 0.35
12s	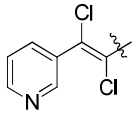	O	>2.0	0.67 ± 0.054	2.4 ± 0.22	13 ± 1.4	0.56 ± 0.034
12t	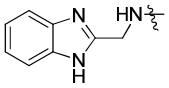	S	>2.0	0.046 ± 0.005	22 ± 2.0	>100	31 ± 4.3
16a	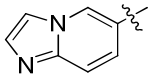	O	>2.0	0.087 ± 0.009	1.8 ± 0.11	46 ± 4.4	5.5 ± 0.47
16b	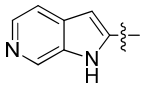	O	>2.0	0.071 ± 0.006	3.3 ± 0.39	41 ± 4.4	4.7 ± 0.53

16c	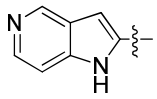	O	>2.0	0.084 ± 0.006	4.0 ± 0.65	48 ± 3.8	1.7 ± 0.14
16d	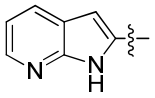	O	>2.0	0.033 ± 0.002	10 ± 2.0	>100	6.1 ± 0.55
16e	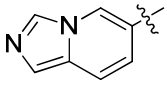	O	>2.0	0.093 ± 0.008	7.4 ± 0.66	54 ± 6.5	3.4 ± 0.42
16f	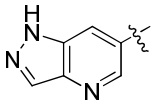	O	>2.0	0.24 ± 0.021	18 ± 2.1	98 ± 9.1	23 ± 0.30
16g	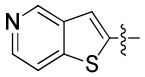	O	>2.0	0.083 ± 0.009	3.0 ± 0.26	40 ± 5.1	0.38 ± 0.022
1			NT[a]	0.026 ± 0.003	3.1 ± 0.22	>100	4.1 ± 0.40
2			0.009 ± 0.0002	NT[a]	1.6 ± 0.12	1.3 ± 0.17	0.89 ± 0.074
5			NT[a]	1.2 ± 0.10	10 ± 2.3	NT[a]	10 ± 3.2
6			0.12 ± 0.02	1.6 ± 0.18	1.0 ± 0.11	NT[a]	4.2 ± 0.37

[a]NT = not tested

Further optimzation efforts were focused on the thiourea group and phenyl linker. When the thiourea group of lead compound **6** was replaced by urea (**12q**) or α,β-unsaturated amide (**12r**), a banlanced NAMPT/HDAC1 inhibitory activity was achieved. Due to the importance of 1,2,3-triazole in the NAMPT inhibitors,[40] a series of 1,2,3-triazole containing derivatives were further synthesized (**24**, **30** and **35**). Interestingly, the insertion of 1,2,3-triazole containing linker led to the increased activity toward both enzymes (**Table 2**). In particular, compound **35** (NAMPT IC_{50} = 0.031 μM, HDAC1 IC_{50} = 0.055 μM) performed the best for the balanced inhibition of NAMPT and HDAC1. Considering that *ortho*-amino anilides were reported to be slow-binders,[38] HDAC1 inhibitory activity was measured after 3 h incubation with

compounds **5** and **35**. As a result, the IC_{50} value of compounds **5** and **35** against HDAC1 was 60 nM and 24 nM, respectively.

Table 2. Enzyme inhibition and *in vitro* antitumor activity of target compounds

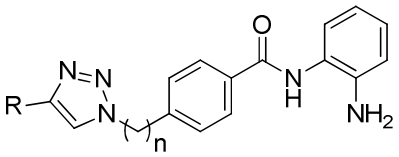

Compds	R	n	IC_{50} (μM)				
			NAMPT	HDAC1	HCT116	MDA-MB-231	HepG2
24		2	0.19 ± 0.021	0.18 ± 0.011	5.5 ± 0.43	41 ± 3.7	3.2 ± 0.33
30	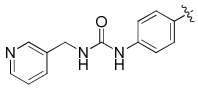	1	0.018 ± 0.001	0.041 ± 0.002	>100	>100	8.1 ± 0.79
35	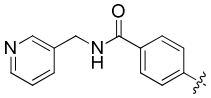	1	0.031 ± 0.009	0.055 ± 0.004	2.4 ± 0.22	10 ± 2.4	4.5 ± 0.35
1			NT[a]	0.026 ± 0.003	3.1 ± 0.22	>100	4.1 ± 0.40
2			0.009 ± 0.0002	NT[a]	1.6 ± 0.12	1.3 ± 0.17	0.89 ± 0.074
5			NT[a]	1.2 ± 0.10	10 ± 2.3	NT[a]	10 ± 3.2
6			0.12 ± 0.02	1.6 ± 0.18	1.0 ± 0.11	NT[a]	4.2 ± 0.37

[a]NT = not tested.

As shown in **Figure 5A**, the binding mode of compound **35** with NAMPT was very similar to that of compounds **2** and **6**. Its pyridinyl group formed face-to-face π-π interactions with Phe193 and Tyr18′, respectively. The amide carbonyl group formed hydrogen bonding interactions with the hydroxyl group of Ser275. Moreover, the terminal *N*-(2-aminophenyl)benzamide projected out of the active site, whose carbonyl group and terminal NH_2 group formed hydrogen bonding interactions with the side chain of Lys189 and the backbone carbonyl group of Asp184, respectively.

The binding mode of compound **35** with HDAC1 was shown in **Figure 5B**. The phenyl linker and terminal phenyl group formed π-π stacking interaction with Phe150 and His141, respectively. Besides chelating with Zn^{2+}, the terminal *N*-(2-aminophenyl)benzamide group was engaged with a hydrogen bonding network with His140, Hisl41 and Gly149. The terminal NH_2 group formed two hydrogen bonds with the nitrogen atom in the imidazole of His140 and Hisl41, respectively. The amide NH group formed hydrogen bonding interaction with the backbone carbonyl group of Gly149. The NH group in head formed hydrogen bonding interaction with the backbone carbonyl group of Glu98.

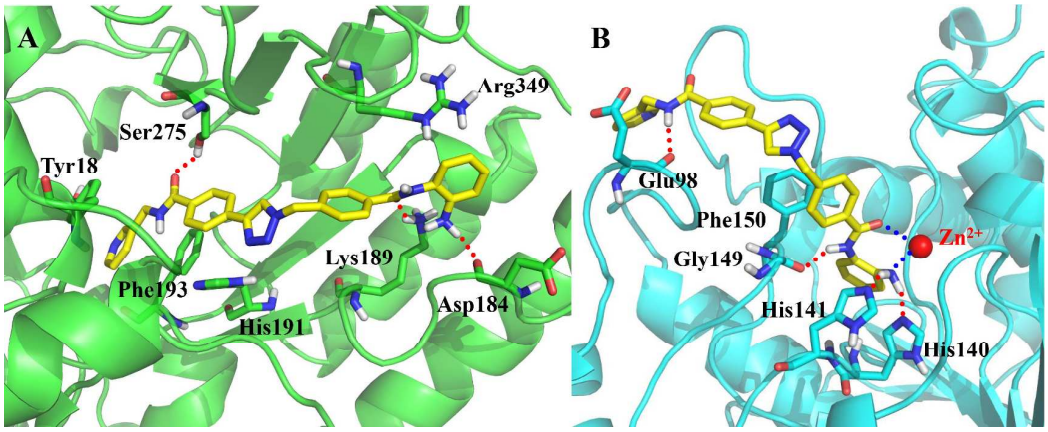

Figure 5. (**A**) Proposed binding mode of compound **35** in the active site of NAMPT (PDB ID: 2GVJ). (**B**) Proposed binding mode of compound **35** in the active site of HDAC1 (PDB ID: 4BKX). The figure was generated using PyMol (http://www.pymol.org/).

In vitro antitumor activity assay revealed that most target compounds showed moderate to good inhibitory activity against the tested three cancer cell lines. In general, compounds are more effective against HCT116 and HepG2 cells than

MDA-MB-231 cells. Most compounds (**12a-p**, **12s-t**, and **16a-g**) seems to act mainly through the inhibition of HDAC, and their *in vitro* antitumor activity was generally consistent with the HDAC inhibitory activities. For example, compound **16g** (NAMPT IC_{50} > 2 μM, HDAC1 IC_{50} = 0.083 μM) showed good activity against HCT116 (IC_{50} = 3.0 μM) and HepG2 (IC_{50} = 0.38 μM) cell lines. For the NAMPT/HDAC1 dual inhibitors, compound **35** showed potent activity against all the tested cell lines particularly for HCT116 cells (IC_{50} = 2.4 μM). Surprisingly, compound **30** was only active against HepG2 cells despite its good activity against both targets. The underlying reasons remain to be further investigated. Considering the enzyme inhibition and antitumor activity, compound **35** was selected for further evaluations.

***In vitro* HDAC Isoform Selectivity of Compound 35.** To obtain evidence for the HDAC isoform selectivity, the inhibitory activity of compound **35** was examined against recombinant HDAC1, HDAC2, HDAC3, HDAC4, HDAC6 and HDAC8 (**Table 3**). As depicted in **Table 3**, compound **35** exhibited remarkable selectivity for HDAC1 and HDAC2 over other isoforms. It showed nanomolar activity against HDAC1 (IC_{50} = 55 nM) and HDAC2 (IC_{50} = 75 nM). In contrast, its activity against HDAC3 (IC_{50} = 1867 nM) was significantly decreased. For other isoforms, such as HDAC6 and HDAC8, compound **35** was totally inactive.

Table 3. HDAC profiling of compound **35** and **1**

		IC_{50} (nM)	
	HDAC class	**1**	**35**
HDAC1	I	26 ± 2.1	55 ± 3.5
HDAC2	I	149 ± 8.5	75 ± 7.4
HDAC3	I	51 ± 4.1	1867 ± 252
HDAC4	IIa	> 100 μM	> 100 μM
HDAC6	IIb	21 ± 1.4	> 100 μM
HDAC8	I	7300 ± 300	> 100 μM

Compound 35 Induces Cell Cycle Arrest, Apoptosis and Autophagy. To investigate whether compound **35** can lead to cell death by apoptosis, an annexin VFITC/propidium iodide (PI) binding assay was performed. Compound **5** was used as a reference drug. HCT116 cells were treated with vehicle alone or tested compounds at 5 μM for 72 h, stained with Annexin V-FITC and PI, and analyzed by flow cytometry. As shown in **Figure 6A**, compound **35** caused significant induction of apoptosis in the HCT116 cell line. The percentage of apoptotic cells for compound **35** was 43.99% (Q2 + Q4), which displayed a higher apoptosis level than compounds **4** and **5** (40.51% and 31.56%, respectively). The result revealed that compound **35** could efficiently induce apoptosis of HCT116 cells and showed synergistic effect at the cellular level.

Western blot assay was performed to determine the autophagic activity induced by compound **35**. HCT116 cells were exposed to compound **35** at 5 μM for 24-72 h. An equivalent volume of DMSO was added as the control. As shown in **Figure 6B**, a significant intratumoral increase in LC3-II level was observed after drug treatment for 24 h compared with the control. However, this kind of increase was followed by a significant reduction at 48 h and 72 h of incubation, suggesting that compound **35**

induced activation of autophagy and increased autophagosome formation at 24 h after drug treatment. To validate the result, P-62 was also measured by Western blot. As depicted in **Figure 6B**, P-62 level was significant decreased at 24 h, 48 h and 72 h of incubation, indicating that compound **35** induced P-62 degradation. Autophagy has been considered as a cytoprotective mechanism, which also has the capacity to promote cell death.[41] Both NAD synthesis inhibition and HDACi could induce autophagy in cancer cells.[42, 43] However, they worked in different ways. Compound **2**-induced autophagy promoted cell death[41], while autophagy induced by **1** functioned as a cytoprotective mechanism. Inhibition of **1**-induced autophagy increased cell apoptosis in glioblastoma stem cells.[44] To illustrate the function of autophagy in **35**-induced cell death, HCT116 cells were incubated with autophagy inhibitor wortmannin for 1 h and subsequently treated with **35** for 72 h. Cell apoptosis was assessed using Annexin V-FITC and PI staining and analyzed by flow cytometry. As shown in **Figure 6A**, inhibition of autophagy by wortmannin dramatically decreased **35**-induced cell apoptosis (43.99% vs 27.68%), suggesting that autophagy induced by **35** promoted cell death in HCT116 cells.

The effect of compound **35** on various phases of cell cycle progression was tested in HCT116 cells (**Figure 6C**). HCT116 cells were treated with vehicle alone or compound **35** at 1 and 5 μM for 48 h, and evaluated by flow cytometric method.[45] The ratios in G2 phase of the cell cycle were 19% at 1 μM and 39% at 5 μM, respectively. In contrast, the ratios of cells untreated in G2 phase of the cell cycle were 5%. In

comparison to the control population, the cell cycle data clearly showed compound **35** arrested HCT116 cells mainly at the G2 phase

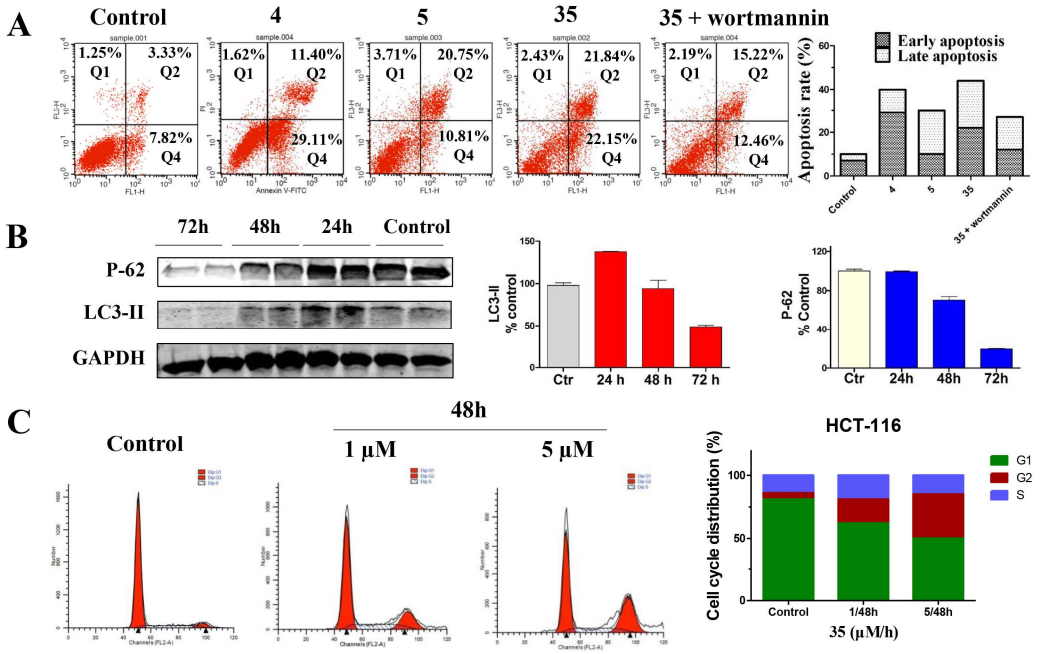

Figure 6. Compound 35 induces apoptosis and autophagy, and arrests cell cycle at G2 phase. (**A**) Cell apoptosis induced by compounds **4**, **5** and **35**. HCT116 cells were treated with **4**, **5** or **35** at 5 μM in the presence or absence of wortmannin (0.25 μM) for 72 h. Apoptosis was examined by flow cytometer. (**B**) Western blot analysis and corresponding quantification of LC3-II and P-62 form in untreated control cells (ctr) and HCT116 cells treated with **35** (5 μM) at different time points. (**C**) Cell cycle analysis after 48 h of treatment. HCT116 cells treated with **35** (at 1 and 5 μM) for 48 h were assayed by flow cytometry after staining with PI.

Compound 35 Inhibits NAMPT and HDAC in HCT116 Cells. The effect of the compound **35** on the acetylation level of histone 3 and histone 4 is shown in **Figure 7A**. Human HCT116 cells were exposed to compound **35** at 1 μM and 5 μM for 24 h. An equivalent volume of DMSO was added as the control. The data showed that compound **35** caused a dramatic increase in acetyl-histone H3 and acetyl-histone H4 in a dose dependent manner. As shown in **Figure 7B**, compound **35** decreased the cellular NAD level effectively after incubation with human cell line HCT116 for 24 h. To verify whether NAMPT is the direct binding target in intact cells, cellular thermal shift assay (CETSA)[22] was performed in HCT116 cells. Treated cells were exposed to compound **35** for 4 h and were harvested. The cell lysates were collected, diluted and heated at different temperatures, which were analyzed by sodium dodecyl sulfate polyacrylamide gel electrophoresis (SDS-PAGE) followed by Western blot. NAMPT protein levels from cells incubated with **35** were more stable as compared with the control, indicating potent binding of **35** with NAMPT (**Figure 7C**). As shown in **Figure 7D**, CESTA melt curves in intact cell for NAMPT target with **35** moved to the right obviously, with the ΔTm value of 1.58 ^{o}C. Thus, NAMPT was confirmed as the direct binding target of **35** in living cells

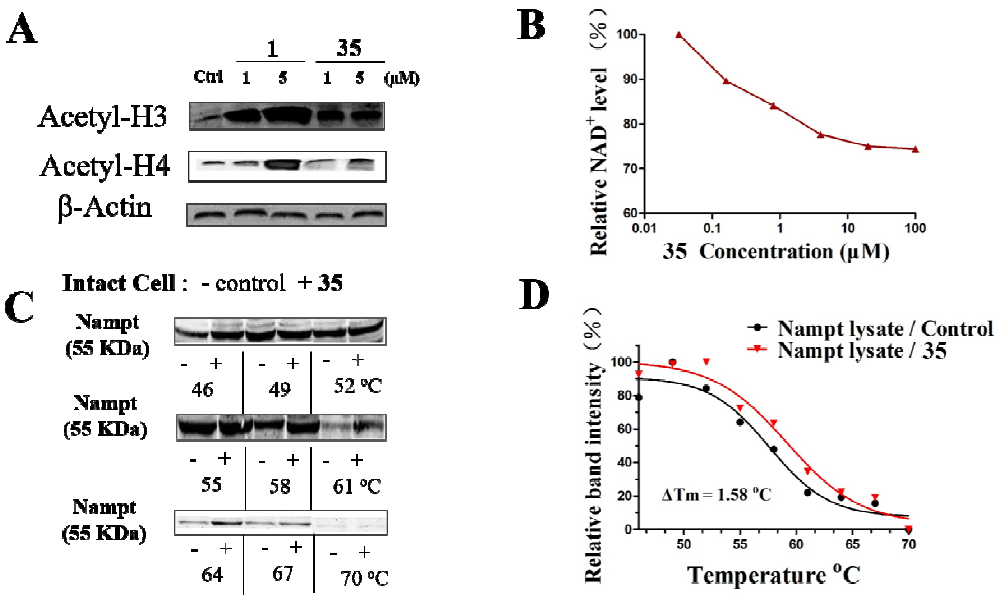

Figure 7. Inhibitory effects of compound 35 against NAMPT and HDAC in HCT116 Cells. (**A**) Western blot analysis of acetylated histone H3 and acetylated histone H4 after 24 h treatment with **35** (at 1 μM and 5 μM) in HCT116 cells. (**B**) Concentration response curve of **35** on NAD level of HCT116 cells after 24 h treatment. (**C**) Western bolt of cellular thermal shift assay in intact cell for NAMPT with compound **35** (at 10 μM). (**D**) CESTA melt curves in intact cells for NAMPT with **35** (at 10 μM).

***In vivo* Antitumor Efficacy and Preliminary PK study of Compound 35.** Compound **35** was chosen to evaluate the *in vivo* antitumor efficacy duo to its excellent and balanced inhibitory activity toward both NAMPT and HDAC1. Initially, PK studies of compounds **1**, **2** and **35** in mice were performed, which were administered intraperitoneally (ip) at 25 mg/kg twice a day (bid). Compound **35** produced high plasma concentration, which was much higher than reference

compounds **1** and **2** (**Figure S7** and **Table S3** in supporting information). Then, HCT116 xenograft nude mouse model was prepared according the procedure described previously.[45] when implanted tumors had reached a volume of 100-300 mm^3, compound **35** was administered intraperitoneally (ip) at 25 mg/kg twice a day for 21 consecutive days. Compounds **1** (25 mg/kg, ip, bid) and **2** (15 mg/kg, ip, bid) were used as the positive control because of their clinical experience.[11, 25] Tumor volumes and body weights were monitored every 3 days over the course of treatment. Tumor growth inhibition (TGI) and relative increment ratio (*T/C*) were calculated at the end of treatment.[46] As shown in **Figure 8A**, treatment with compound **35** caused a dramatic reduction in tumor growth. Moreover, compound **35** demonstrated much higher antitumor activity (TGI = 69%, *T/C* = 31%) than the reference drug **1** (TGI = 33%, *T/C* = 67%) and **2** (TGI = 39%, *T/C* = 61%). The final tumor tissue size visualized in **Figure 8B** also explicitly showed an excellent antineoplastic activity of compound **35**. These finding demonstrated that dual NAMPT/HDAC inhibitor led to improved *in vivo* antitumor potency as compared with single HDAC or NAMPT inhibitor. The PK profile of compound **35** was further investigated. It was administered ip at 2 mg/kg in Sprague-Dawley (SD) rats (**Figure S8** in supporting information). The terminal half-life of **35** was approximately 1.8 h. The peak concentration C_{max}, plasma clearance (Cl) and the volume of distribution absorption (V_{ss}) was 745 ng/mL, 6173 mL/h/kg and 6229 mL/kg, respectively (**Table S2**). The results indicated that the PK properties of compound **35** remain to be further improved to achieve better *in vivo* antitumor activities.

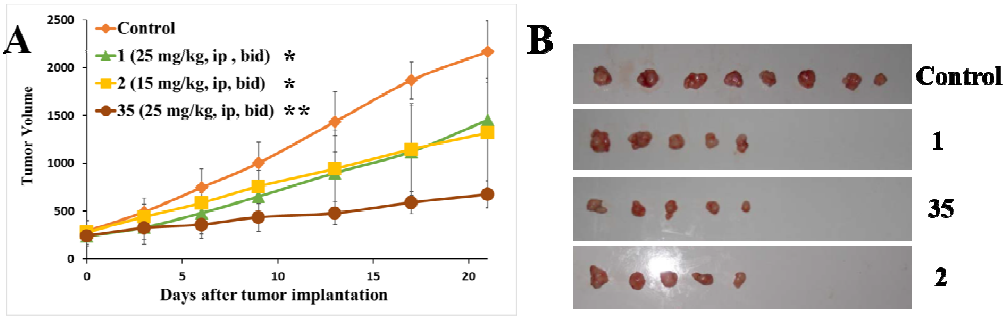

Figure 8. Growth curve of implanted HCT116 xenograft in nude mice. (**A**) *In vivo* efficacy of compound **35** in HCT116 tumor xenograft model. Data are expressed as the mean ± standard deviation. * $P < 0.05$, ** $P < 0.01$, versus the control group, determined with Student's *t* test. (**B**) Picture of dissected HCT116 tumor tissues.

CONCLUSION

In summary, the present investigation provides a proof-of-concept study of discovering dual NAMP/HDAC inhibitors. The first dual NAMPT/HDAC inhibitors were rationally designed and optimized on the basis of the structural features of both NAMPT and HDAC inhibitors. In particular, compound **35** possessed the best balanced activities against both NAMPT and HDAC. Interestingly, compound **35** can effectively induce the apoptosis and autophagy of HCT116 cells, which may relate to enhanced antitumor activity and ultimately lead to cell death. Antitumor mechanism and target profiling study indicated that compound **35** acted by direct inhibition of both NAMPT and HDAC in living cells. Importantly, compound **35** showed excellent *in vivo* antitumor efficacy in HCT116 xenograft models (TGI = 69%, 25 mg/kg, ip, bid), which was much more effective than HDAC inhibitor **1** and NAMPT inhibitor **2**. The results highlighted the advantages of dual NAMPT/HDAC inhibitors as novel

antitumor agents and provided an efficient strategy for multi-target antitumor drug discovery. Compound **35** represented a promising lead compound for the development of novel antitumor agent. It also should be noted that thrombocytopenia is the common side effect of both NAMPT and HDAC inhibitors observed in the clinic trials.[20, 47] However, thrombocytopenia in HDAC inhibitors is transient and reversible, which disappears shortly after removal of the agent with platelet counts recovering rapidly after treatment is stopped.[47] The enzyme inhibitory activity of dual NAMPT/HDAC inhibitor **35** was weaker than that of **1** and **2**, respectively. Thus, whether this kind of dual inhibition can reduce the thrombocytopenia side effect remains to be further investigated. Moreover, the PK profiles of compound **35** still need to be improved and its therapeutic advantages over the combination of a NAMPT inhibitor and an HDAC inhibitor remain to be further investigated. Such structural optimization studies are in progress.

EXPERIMENTAL SECTION

General. Reagents were purchased from commercial sources and were used without further purification. Oxygen or water sensitive reactions were performed under the nitrogen atmosphere. ^{13}C-NMR and ^{1}H-NMR spectra were recorded on Bruker AVANCE600, or AVANCE300 spectrometer (Bruker Company, Germany), operating at the indicated frequencies and $CDCl_3$ or DMSO-d_6 as solvents. Chemical shift was expressed in ppm (δ). The mass spectra were recorded on an Esquire 3000 LC-MS mass spectrometer. Flash chromatography was performed on 200-300 mesh silica gel

with the indicated solvent systems (Qingdao Haiyang Chemical, China). Chemical purities were analyzed by HPLC using MeOH/H_2O as the mobile phase with a flow rate of 0.6 mL/min on a C18 column. All final compounds exhibited the purity greater than 95%.

***N*-(2-aminophenyl)-4-(3-((6-fluoropyridin-3-yl)methyl)thioureido)benzamide (12a).** 6-Fluoro-3-cyanopyridine (300 mg, 2.46 mmol) was dissolved in the ammonia/MeOH solution (30 mL, 2 mol/L) and stirred at room temperature. Raney Ni (0.5 g) was added to the reaction mixture, and then stirred for 12 h at room temperature under the H_2 atmosphere. The reaction mixture was filtered through diatomite, washed with MeOH (5 mL × 2). The filtrate was concentrated in vacuo and purified by silica gel column chromatography (CH_2Cl_2 : MeOH = 100 : 2) to give intermediate **8** (R_1 = F, R_2 = H, 0.264 g, 85%) as a white yellow oil.[48] ^{1}H-NMR (DMSO-d_6, 300 MHz) δ: 8.11-6.84 (m, 3H), 3.86 (s, 2H), 1.47 (s, 2H).

To a stirred solution of 4-aminobenzoic acid (1.25 g, 11.57 mmol) and Et_3N (1.4 mL, 194 mmol) in CH_2Cl_2 (12 mL) was added 1,1'-thiocarbonyldiimidazole (2.11 g, 11.85 mmol), and the mixture was stirred under ice bath for 1 h. Then hydrochloric acid (3 mL, 33.60 mmol) in hexane (12 mL) was added to the reaction solution, and stirred at room temperature for 2 h. Then, the mixture was diluted in ice water, and the precipitate was filtered off. The residue was dried to give a gray white intermediate **10** (X = S, 1.93 g, yield 93 %) without further purification. ^{1}H-NMR (DMSO-d_6, 300 MHz) δ: 13.20 (br s, 1H), 7.52 (d, J = 8.7 Hz, 2H), 7.97 (d, J = 8.7 Hz, 2H).

A solution of compound **8** (R_1 = F, R_2 = H, 133 mg, 1.06 mmol) and **10** (X = S, 189

mg, 1.06 mmol) in dry THF (10 mL) was stirred at room temperature for 12 h. Then the mixture was concentrated in vacuo to give product **11a** (0.26 g, 81%) as a yellow solid. ^{1}H-NMR (DMSO-d_6, 300 MHz) δ: 10.24 (s, 1H), 8.75 (s, 1H), 8.36-8.34 (m, 2H), 7.87 (d, J = 8.5 Hz, 2H), 7.63-7.58 (m, 3H), 4.80 (d, J = 5.4 Hz, 2H). ESI-MS (m/s): 287.12 [M+1].

To a solution of compound **11a** (90 mg, 0.30 mmol), HBTU (114 mg, 0.30 mmol) and Et_3N (41 μL, 0.30 mmol) in DMF (5 mL) was added *o*-phenylenediamine (32 mg, 0.30 mmol), and the mixture was stirred at room temperature for 3 h. The reaction solution was diluted with water (40 mL) and filtered. The precipitate was dried and purified by column chromatography (CH_2Cl_2 : MeOH = 100 : 3) to give target compound **12a** (59 mg, 51%) as a yellow solid. ^{1}H-NMR (DMSO-d_6, 300 MHz) δ: 9.95 (s, 1H), 9.56 (s, 1H), 8.46 (s, 1H), 8.22 (s, 1H), 8.04-7.88 (m, 3H), 7.58 (d, J = 8.3 Hz, 2H), 7.24-7.10 (m, 2H), 6.96 (t, J = 7.1 Hz, 1H), 6.85-6.72 (m, 1H), 6.58 (t, J = 7.3 Hz, 1H), 4.99-4.72 (m, 4H). ESI-MS (m/s): 396.38 [M+1], 394.17 [M-1].

Compounds **12b-t** were synthesized according to a similar protocol described for **12a**.

***N*-(2-Aminophenyl)-4-(3-((6-chloropyridin-3-yl)methyl)thioureido)benzamide (12b).** Yield 64%, yellow solid. ^{1}H-NMR (DMSO-d_6, 300 MHz) δ: 9.98 (s, 1H), 9.59 (s, 1H), 8.52-8.42 (m, 1H), 8.38 (d, J = 2.3 Hz, 1H), 7.94 (d, J = 8.6 Hz, 2H), 7.84 (dd, J = 8.2, 2.4 Hz, 1H), 7.58 (d, J = 8.7 Hz, 2H), 7.50 (d, J = 8.3 Hz, 1H), 7.15 (d, J = 7.4 Hz, 1H), 6.96 (t, J = 7.5 Hz, 1H), 6.77 (d, J = 8.0 Hz, 1H), 6.59 (t, J = 7.2 Hz, 1H), 4.87 (s, 1H), 4.76 (d, J = 5.7 Hz, 2H). ^{13}C-NMR (DMSO-d_6, 150 MHz) δ: 181.89, 165.71, 150.13, 149.73, 144.15, 143.11, 140.10, 135.24, 130.78, 129.42, 127.69,

127.44, 124.95, 124.46, 122.90, 117.30, 117.17, 45.02. ESI-MS (m/s): 412.18 [M+1], 410.12 [M-1].

***N*-(2-Aminophenyl)-4-(3-((6-chloropyridin-3-yl)methyl)ureido)benzamine (12c).** Yield 57%, yellow solid. ^{1}H-NMR (DMSO-d_6, 300 MHz) δ: 9.49 (s, 1H), 9.00 (s, 1H), 8.36 (d, J = 2.1 Hz, 1H), 7.87 (d, J = 8.7 Hz, 2H), 7.79 (dd, J = 8.3, 2.4 Hz, 2H), 7.54-7.46 (m, 3H), 7.13 (d, J = 7.6 Hz, 1H), 7.00-6.90 (m, 1H), 6.86 (t, J = 6.0 Hz, 1H), 6.79-6.73 (m, 1H), 6.58 (t, J = 7.7 Hz, 1H), 4.85 (s, 2H), 4.32 (d, J = 5.8 Hz, 2H). ^{13}C-NMR (DMSO-d_6, 150 MHz) δ: 165.27, 155.47, 149.32, 149.12, 143.77, 143.54, 139.35, 135.97, 129.19, 127.44, 127.05, 126.72, 124.46, 124.16, 117.19, 116.78, 116.65, 46.28. ESI-MS (m/s): 396.17 [M+1].

***N*-(2-Aminiphenyl)-4-(3((6-fluoropyridin-3yl)methyl)ureido)benzamide (12d).** Yield 60%, yellow solid. ^{1}H-NMR (DMSO-d_6, 300 MHz) δ: 9.49 (s, 1H), 9.01 (s, 1H), 8.17 (s, 1H), 7.97-7.83 (m, 3H), 7.50 (d, J = 8.5 Hz, 2H), 7.20-7.10 (m, 2H), 6.98-6.83 (m, 2H), 6.79-6.73 (m, 1H), 6.58 (t, J = 7.7 Hz, 1H), 4.85 (s, 2H), 4.32 (d, J = 5.8 Hz, 2H). ^{13}C-NMR (DMSO-d_6, 150 MHz) δ: 165.28, 155.49, 146.79, 146.69, 143.54, 141.84, 141.79, 129.20, 127.38, 127.05, 126.71, 124.17, 117.14, 116.78, 116.65, 109.79, 109.54, 53.54. ESI-MS (m/s): 380.32 [M+1], 378.24 [M-1].

***N*-(2-Aminophenyl)-4-(3-((6-aminopyridin-3-yl)methyl)thioureido)benzamide (12e).** Yield 52%, light yellow solid. ^{1}H-NMR (DMSO-d_6, 600 MHz) δ: 9.75 (s, 1H), 9.56 (s, 1H), 8.20 (br s, 1H), 7.95-7.88 (m, 3H), 7.60 (d, J = 8.7 Hz, 2H), 7.41 (dd, J = 8.4, 2.2 Hz, 1H), 7.15 (d, J = 6.8 Hz, 1H), 6.97-6.93 (m, 1H), 6.76 (dd, J = 8.0, 1.3 Hz, 1H), 6.58 (dd, J = 7.5, 1.2 Hz, 1H), 6.43-6.41 (m, 1H), 5.88 (s, 2H), 4.87 (s, 2H), 4.52

(d, J = 5.2 Hz, 2H). ^{13}C-NMR (DMSO-d_6, 150 MHz) δ: 180.63, 165.20, 159.52, 147.74, 143.57, 142.92, 137.84, 129.83, 128.77, 127.11, 126.85, 123.96, 121.93, 121.77, 116.76, 116.62, 108.16, 45.20. ESI-MS (m/s): 393.25 [M+1], 391.08 [M-1].

***N*-(2-Aminophenyl)-4-(3-((6-aminopyridin-3-yl)methyl)ureido)benzamide (12f).** Yield 51%, yellow solid. ^{1}H-NMR (DMSO-d_6, 300 MHz) δ: 9.48 (s, 1H), 8.85 (s, 1H), 7.92-7.82 (m, 3H), 7.50 (d, J = 8.7 Hz, 2H), 7.50 (d, J = 8.8 Hz, 2H), 7.34 (dd, J = 8.7, 2.4 Hz, 1H), 7.14 (dd, J = 7.9, 1.2 Hz, 1H), 7.00-6.90 (m, 1H), 6.80-6.73 (m, 1H), 6.70-6.54 (m, 2H), 6.42 (d, J = 8.5 Hz, 1H), 5.86 (s, 2H), 4.86 (br s, 2H), 4.09 (d, J = 5.5 Hz, 2H). ^{13}C-NMR (DMSO-d_6, 75 MHz) δ: 165.31, 159.33, 158.72, 158.31, 155.43, 147.16, 144.12, 143.55, 137.46, 129.17, 127.06, 126.68, 124.15, 123.47, 119.58, 116.91, 116.73, 116.61, 115.62, 108.20, 49.04. ESI-MS (m/s): 377.13[M+1].

***N*-(2-Aminophenyl)-4-(3-((5-fluoropyridin-3-yl)methyl)thioureido)benzamide (12h).** Yield 67%, yellow solid. ^{1}H-NMR (DMSO-d_6, 300 MHz) δ: 10.00 (s, 1H), 9.59 (s, 1H), 8.59-8.41 (m, 3H), 7.94 (d, J = 8.5 Hz, 2H), 7.72-7.65 (m, 1H), 7.59 (d, J = 8.6 Hz, 2H), 7.14 (d, J = 7.4 Hz, 1H), 6.96 (t, J = 7.6 Hz, 1H), 6.77 (d, J = 7.0 Hz, 1H), 6.59 (t, J = 7.0 Hz, 1H), 4.96-4.77 (m, 4H). ^{13}C-NMR (DMSO-d_6, 150 MHz) δ: 182.00, 165.72, 146.22, 146.17, 144.10, 143.15, 137.29, 136.99, 130.78, 129.41, 127.68, 127.43, 124.49, 123.15, 122.91, 117.34, 117.19, 45.19. ESI-MS (m/s): 396.21 [M+1], 394.12 [M-1].

***N*-(2-Aminophenyl)-4-(3-((6-methylpyridin-3-yl)methyl)thioureido)benzamide (12i).** Yield 57%, yellow solid. ^{1}H-NMR (DMSO-d_6, 300 MHz) δ: 9.89 (s, 1H), 9.58 (s, 1H), 8.48-8.36 (m, 2H), 7.93 (d, J = 8.6 Hz, 2H), 7.66 (dd, J = 7.9, 2.3 Hz, 1H),

7.59 (d, *J* = 8.6 Hz, 2H), 7.23 (d, *J* = 8.0 Hz, 1H), 7.15 (d, *J* = 6.9 Hz, 1H), 6.96 (dd, *J* = 8.0, 1.3 Hz, 1H), 6.77 (d, *J* = 6.9 Hz, 1H), 6.59 (t, *J* = 7.6 Hz, 1H), 4.90 (br s, 2H), 4.72 (d, *J* = 5.5 Hz, 2H), 2.44 (s, 3H). ^{13}C-NMR (DMSO-d_6, 150 MHz) δ: 181.18, 165.18, 159.92, 148.74, 143.57, 142.74, 136.22, 131.71, 130.06, 128.82, 127.11, 126.86, 123.95, 123.14, 122.10, 116.77, 116.63, 45.03, 24.15. ESI-MS (m/s): 392.32 [M+1], 390.15 [M-1].

***N*-(2-Aminophenyl)-4-(3-(4-fluorobenzyl)thioureido)benzamime (12k).** Yield 60%, yellow solid. ^{1}H-NMR (DMSO-d_6, 300 MHz) δ: 9.85 (s, 1H), 9.55 (s, 1H), 8.36 (s, 1H), 7.89 (d, *J* = 8.0 Hz, 2H), 7.57 (d, *J* = 8.0 Hz, 2H), 7.41-7.29 (m, 1H), 7.20-7.03 (m, 3H), 6.97-6.85 (m, 1H), 6.73 (d, *J* = 7.6 Hz, 1H), 6.55 (t, *J* = 7.2 Hz, 1H), 5.01-4.55 (m, 4H). ^{13}C-NMR (DMSO-d_6, 75 MHz) δ: 181.12, 165.19, 143.56, 142.83, 135.43, 130.05, 130.00, 128.79, 127.11, 126.86, 123.95, 121.99, 116.77, 116.63, 115.57, 115.43, 46.85. ESI-MS (m/s): 395.12 [M+1], 393.05 [M-1].

***N*-(2-Aminophenyl)-4-(3-(2-fluorobenzyl)thioureido)benzamime (12m).** Yield 70%, yellow solid. ^{1}H-NMR (DMSO-d_6, 300 MHz) δ: 10.02 (s, 1H), 9.58 (s, 1H), 8.49-8.32 (m, 1H), 7.93 (d, *J* = 8.5 Hz, 2H), 7.66 (d, *J* = 8.5 Hz, 2H), 7.47-7.27 (m, 2H), 7.24-7.10 (m, 2H), 6.96 (dd, *J* = 8.0, 1.4 Hz, 1H), 6.77 (dd, *J* = 7.8, 0.9 Hz, 1H), 6.59 (t, *J* = 7.7 Hz, 1H), 4.88 (br s, 2H), 4.79 (d, *J* = 5.1 Hz, 2H). ^{13}C-NMR (DMSO-d_6, 75 MHz) δ: 181.86, 165.75, 144.15, 143.49, 130.73, 130.44, 130.12, 130.01, 129.32, 127.68, 127.40, 125.37, 125.32, 124.50, 117.28, 117.16, 116.28, 116.00, 42.01. ESI-MS (m/s): 395.05 [M+1], 392.86 [M-1].

***N*-(2-Aminophenyl)-4-(3-(benzo[*d*][1,3]dioxol-5-ylmethyl)thioureido)benzamide**

(12o). Yield 43%, yellow solid. ^{1}H-NMR (DMSO-d_6, 600 MHz) δ: 9.82 (s, 1H), 9.57 (s, 1H), 8.29 (s, 1H), 7.95-7.90 (m, 2H), 7.61 (d, J = 8.8 Hz, 2H), 7.16-7.12 (m, 1H), 6.97-6.93 (m, 2H), 6.89-6.85 (m, 1H), 6.85-6.81 (m, 1H), 6.77 (dd, J = 8.0, 1.3 Hz, 1H), 6.58 (dd, J = 7.7, 1.5 Hz, 1H), 5.99 (s, 2H), 4.87 (br s, 2H), 4.66-4.61 (m, 2H). ^{13}C-NMR (DMSO-d_6, 75 MHz) δ: 181.06, 165.33, 147.84, 146.87, 143.71, 143.02, 133.07, 130.06, 128.91, 127.25, 126.99, 124.10, 122.03, 121.55, 116.89, 116.76, 108.87, 108.70, 101.48, 47.57. ESI-MS (m/s): 421.16 [M+1], 419.08 [M-1].

4-(3-(3-Aminobenzyl)thioureido)-*N*-(2-aminophenyl)benzamide (12p). Yield 75%, light yellow solid. ^{1}H-NMR (DMSO-d_6, 600 MHz) δ: 9.78 (s, 1H), 9.54 (s, 1H), 8.20 (s, 1H), 7.92 (d, J = 8.6 Hz, 2H), 7.66 (d, J = 8.6 Hz, 2H), 7.16 (d, J = 7.4 Hz, 1H), 7.01-6.92 (m, 2H), 6.77 (dd, J = 8.0, 1.2 Hz, 1H), 6.59 (dd, J = 8.0, 1.2 Hz, 1H), 6.54 (s, 1H), 6.50-6.44 (m, 2H), 5.05 (s, 2H), 4.85 (s, 2H), 4.59 (d, J = 4.7 Hz, 2H). ^{13}C-NMR (DMSO-d_6, 150 MHz) δ: 180.97, 165.35, 149.38, 143.70, 143.16, 139.57, 129.93, 129.49, 128.89, 127.23, 126.98, 124.13, 121.79, 116.90, 116.77, 115.63, 113.53, 113.37, 48.23. ESI-MS (m/s): 392.20 [M+1], 390.12 [M-1].

***N*-(2-Aminophenyl)-4-(3-(pyridin-3-yl)acrylamido)benzamide (12r).** Yield 44%, yellow solid. ^{1}H-NMR (DMSO-d_6, 300 MHz) δ: 10.57 (s, 1H), 9.60 (s, 1H), 8.85 (s, 1H), 8.61 (s, 1H), 8.15-7.94 (m, 3H), 7.92-7.77 (m, 2H), 7.75-7.63 (m, 1H), 7.51 (s, 1H), 7.17 (s, 1H), 7.08-6.89 (m, 2H), 6.79 (s, 1H), 6.61 (s, 1H), 4.90 (s, 2H). ^{13}C-NMR (DMSO-d_6, 75 MHz) δ: 165.18, 163.90, 151.01, 149.82, 143.59, 142.35, 137.90, 134.68, 130.92, 129.79, 129.25, 127.11, 126.84, 124.55, 124.44, 123.96, 118.95, 116.75, 116.61. ESI-MS (m/s): 359.17 [M+1], 357.30 [M-1].

***N*-(4-((2-Aminophenyl)carbamoyl)benzyl)imidazo[1,2-*a*]pyridine-7-carboxamide (16a).** A solution of imidazo[1,2-*a*]pyridine-6-carboxylic acid (200 mg, 1.00 mmol), EDC (230 mg, 1.00 mmol) and DMAP (146 mg, 1.20 mmol) in DMF (5 mL) was stirred at room temperature for 0.5 h. Methyl 4-(aminomethyl)benzoate (165 mg, 1.00 mmol) was added, and the mixture was stirred at room temperature for another 3 h. The mixture was diluted with water (40 mL), and extracted with EtOAc (50 mL × 3). The combined organic layers were dried over $MgSO_4$, concentrated and purified by silica gel column chromatography (CH_2Cl_2 : MeOH = 100 : 2) to give compound **14a** (120 mg, 34%) as a yellow solid. ^{1}H-NMR (DMSO-d_6, 300 MHz) δ: 9.21 (t, J = 5.7 Hz, 1H), 9.16 (s, 1H), 8.08 (s, 1H), 7.90 (d, J = 8.3 Hz, 2H), 7.73-7.60 (m, 3H), 7.44 (d, J = 8.4 Hz, 2H), 4.57 (d, J = 5.8 Hz, 2H), 3.84 (s, 3H). ESI-MS (m/s): 310.51 [M+1], 300.23 [M-1].

A solution of intermediate **14a** (120 mg, 0.387 mmol) and LiOH (28 mg, 1.16 mmol) in the mixed solvent THF/MeOH/H_2O (3:2:1, v/v, 6 mL) was stirred at room temperature for 24 h. The solution was concentrated and then diluted in water (10 mL). The pH value of the mixture was adjusted to 3-4 by 2 M hydrochloric acid. The resulting precipitate was collected by filtration to give target compound **15a** (111 mg, 97%) as a white solid. ^{1}H-NMR (DMSO-d_6, 300 MHz) δ: 12.92 (br s, 1H), 9.22 (t, J = 5.7 Hz, 1H), 9.17 (s, 1H), 8.08 (s, 1H), 7.91 (d, J = 8.3 Hz,2H), 7.72-7.60 (m, 3H), 7.45 (d, J = 8.3 Hz, 2H), 4.57 (d, J = 5.7 Hz, 2H). ESI-MS(m/s): 296.42 [M+1], 294.19 [M-1].

To a stirred solution of compound **15a** (111 mg, 0.38 mmol), HBTU (157 mg, 0.41

mmol) and Et_3N (60 μL, 0.41 mmol) in DMF (5 mL) was added *o*-phenylenediamine (45 mg, 0.41 mmol), and the reaction mixture was stirred at room temperature for 4 h. The mixture was poured into water (40 mL), and filtered to give the crude product, which was purified by column chromatography (CH_2Cl_2 : MeOH = 100 : 3) to give target compound **16a** (56 mg, 38%) as a white solid. ^{1}H-NMR (DMSO-d_6, 300 MHz) δ: 9.62 (s, 1H), 9.22 (t, J = 6.1 Hz, 1H), 9.17 (s, 1H), 8.08 (s, 1H), 7.94 (d, J = 8.4 Hz, 2H), 7.77-7.57 (m, 3H), 7.45 (d, J = 8.2 Hz, 2H), 7.15 (d, J = 7.6 Hz, 1H), 6.95 (t, J = 6.9 Hz, 1H), 6.76 (d, J = 7.1 Hz, 1H), 6.58 (t, J = 7.4 Hz, 1H), 4.57 (d, J = 4.6 Hz, 2H). ^{13}C-NMR (DMSO-d_6, 150 MHz) δ: 165.57, 164.76, 144.84, 143.55, 143.38, 143.26, 134.37, 133.68, 129.15, 128.27, 127.80, 127.63, 127.15, 126.94, 124.97, 123.79, 123.66, 120.24, 119.59, 116.74, 116.60, 116.40, 114.92, 110.07, 49.06, 42.96.ESI-MS (m/s): 386.38 [M+1], 384.30 [M-1].

Compounds **16b-g** were synthesized according to a similar protocol described for **16a**.

***N*-(4-((2-Aminophenyl)carbamoyl)benzyl)-1*H*-pyrrolo[2,3-*c*]pyridine-2-carboxa mide (16b).** Yield 52%, yellow solid. ^{1}H-NMR (DMSO-d_6, 300 MHz) δ: 12.22 (s, 1H), 9.64 (s, 1H), 9.48-9.38 (m, 1H), 8.81 (s, 1H), 8.13 (d, J = 5.6Hz, 1H), 7.95 (d, J = 8.1 Hz, 2H), 7.65 (d, J = 5.5 Hz, 1H), 7.51-7.41 (m, 2H), 7.25 (s, 1H), 7.15 (d, J = 7.9 Hz, 1H), 6.95 (dd, J = 8.0, 1.5 Hz, 1H), 6.80-6.74 (m, 1H), 6.58 (t, J = 7.6 Hz, 1H), 4.60 (d, J = 5.9 Hz, 2H). ^{13}C-NMR (DMSO-d_6, 75 MHz) δ: 166.12, 161.51, 144.13, 143.81, 138.26, 136.52, 136.25, 134.29, 134.14, 132.72, 128.95, 128.03, 127.71, 127.45, 124.39, 120.09, 117.27, 117.17, 102.81, 43.14. ESI-MS (m/s): 386.35 [M+1], 384.33 [M-1].

***N*-(4-((2-Aminophenyl)carbamoyl)benzyl)-1*H*-pyrrolo[3,2-*c*]pyridine-2-carboxa mide (16c).** Yield 60%, white solid. ^{1}H-NMR (DMSO-d_6, 300 MHz) δ: 9.63 (s, 1H), 9.32 (t, J = 6.3 Hz, 1H), 8.93 (s, 1H), 8.21 (d, J = 5.7 Hz, 1H), 7.95 (d, J = 8.0 Hz, 2H), 7.45 (d, J = 8.2 Hz, 2H), 7.40-7.31 (m, 3H), 7.15 (d, J = 8.3 Hz, 1H), 6.95 (t, J = 6.6 Hz, 1H), 6.99-6.92 (m, 1H), 6.58 (t, J = 7.5 Hz, 1H), 4.87 (s, 1H), 4.59 (d, J = 5.7 Hz, 2H). ^{13}C-NMR (DMSO-d_6, 75 MHz) δ: 166.13, 161.72, 145.91, 144.15, 143.94, 142.45, 140.57, 134.28, 133.86, 128.93, 127.99, 127.70, 127.49, 125.42, 124.35, 117.28, 117.15, 108.41, 102.99, 43.08. ESI-MS (m/s): 386.39 [M+1], 384.30 [M-1].

***N*-(4-((2-Aminophenyl)carbamoyl)benzyl)-1*H*-pyrrolo[2,3-*b*]pyridine-2-carboxa mide (16d).** Yield 75%, white solid. ^{1}H-NMR (DMSO-d_6, 300 MHz) δ: 12.12 (s, 1H), 9.62 (s, 1H), 9.15 (t, J = 6.0 Hz, 1H), 8.33 (dd, J = 4.6, 1.3 Hz, 1H), 8.10 (d, J = 7.1 Hz, 1H), 7.95 (d, J = 8.1 Hz, 2H), 7.46 (d, J = 8.1 Hz, 2H), 7.18-7.08 (m, 3H), 6.96 (t, J = 7.1 Hz, 1H), 6.81-6.72 (m, 1H), 6.58 (t, J = 6.9 Hz, 1H), 4.88 (s, 2H), 4.58 (d, J = 6.0 Hz, 2H). ^{13}C-NMR (DMSO-d_6, 150 MHz) δ: 165.58, 161.22, 148.85, 145.81, 143.55, 143.45, 133.74, 132.50, 130.50, 128.35, 127.50, 127.19, 126.92, 123.83, 119.77, 116.90, 116.75, 116.61, 102.32, 42.56. ESI-MS (m/s): 386.40 [M+1], 384.38 [M-1].

***N*-(4-((2-Aminophenyl)carbamoyl)benzyl)imidazo[1,5-*a*]pyridine-6-carboxamide (16e).** Yield 48%, white solid. ^{1}H-NMR (DMSO-d_6, 300 MHz) δ: 9.62 (s, 1H), 9.16 (t, J = 5.76 Hz), 8.95 (s, 1H), 8.51 (s, 1H), 7.94 (d, J = 8.1 Hz, 2H), 7.60 (d, J = 9.5 Hz, 1H), 7.50-7.39 (m, 3H), 7.24-7.12 (m, 2H), 7.00-6.91 (m, 1H), 6.79-6.73 (m, 1H), 6.59 (t, J = 7.7 Hz, 1H), 4.88 (br s, 2H), 4.55 (d, J = 5.8 Hz, 2H). ^{13}C-NMR

(DMSO-d_6, 150 MHz) δ: 165.60, 164.97, 143.56, 143.41, 133.72, 130.39, 129.84, 128.34, 127.52, 127.13, 126.93, 125.72, 123.85, 120.28, 120.07, 118.05, 117.79, 116.77, 116.63, 42.95. HRMS (ESI, negative) m/z calcd for $C_{22}H_{18}N_5O_2$ (M - H): 384.1471; found 384.1484.

***N*-(4-((2-Aminophenyl)carbamoyl)benzyl)-1*H*-indazole-6-carboxamide (16f).** Yield 54%, yellow solid. ^{1}H-NMR (DMSO-d_6, 300 MHz) δ: 13.91 (s, 1H), 9.63 (s, 1H), 9.30 (t, J = 5.9 Hz, 1H), 9.03 (d, J = 1.9 Hz, 1H), 8.76 (d, J = 1.9 Hz, 1H), 8.29 (s, 1H), 8.94 (d, J = 8.1 Hz, 2H), 7.47 (d, J = 8.1 Hz, 2H), 7.22-7.12 (m, 2H), 7.00-6.91 (m, 1H), 6.80-6.70 (m, 1H), 6.58 (t, J = 7.5 Hz, 1H), 4.89 (br s, 2H), 4.59 (d, J = 5.7 Hz, 2H). ^{13}C-NMR (DMSO-d_6, 75 MHz) δ: 166.34, 166.15, 153.46, 149.50, 144.10, 135.66, 134.22, 130.83, 128.89, 128.06, 127.68, 127.48, 124.44, 124.46, 117.37, 117.21, 114.67, 43.54, 39.27. ESI-MS (m/s): 387.29 [M+1], 385.35 [M-1].

Methyl 4-(2-(4-(pyridin-3-yl)-1*H*-1,2,3-triazol-1-yl)ethyl)benzoate (22). To a solution of methyl 4-(2-bromoethyl)benzoate methyl ester (364 mg, 1.5 mmol) in DMF (5 mL) was added NaN_3 (195 mg, 3 mmol) slowly at room temperature. Then, the reaction mixture was stirred at 80 ^{o}C for 8 h. The reaction mixture was diluted with water (50 mL), and extracted with EtOAc (50 mL × 3). The combined organic layers were dried over $MgSO_4$, concentrated under reduced pressure to yield compound **21** (261 mg, 85%) as a yellow solid. The crude compound was used directly in the next step without further purification. ^{1}H-NMR (DMSO-d_6, 300 MHz) δ: 7.90 (d, J = 8.3 Hz, 2H), 7.43 (d, J = 8.3 Hz, 2H), 3.83 (s, 3H), 3.77 (t, J = 7.0 Hz, 2H), 3.20 (t, J = 7.0 Hz, 2H). ESI-MS (m/s): 206.35 [M+1].

A solution of 3-ethynyl pyridine[29] (154 mg, 1.5 mmol), compound **21** (307 mg, 1.5 mmol), VcNa (30 mg, 0.15 mmol) and $CuSO_4 \cdot 5H_2O$ (3.8 mg, 0.015 mmol) in the mixed solvent *t*-butanol/H_2O (1:1, v/v, 6 mL) was stirred at room temperature under the N_2 protection for 12 h. Then, the mixture was poured into water (30 mL) and filtered. The precipitate was purified by column chromatography (Hexane : EtOAc = 1 : 2) to give compound **22** (378 mg, 82%) as a white solid. ^{1}H-NMR (DMSO-d_6, 300Hz) δ: 9.04 (d, *J* = 1.7 Hz, 1H), 8.79 (s, 1H), 8.53 (dd, *J* = 4.7, 1.5 Hz, 1H), 8.21 (dd, *J* = 7.9, 1.8 Hz, 1H), 7.97 (d, *J* = 8.2 Hz, 2H), 7.49-7.43 (m, 3H), 5.78 (s, 2H), 3.83 (s, 3H). ESI-MS (m / s): 309.35 [M + 1].

***N*-(2-Aminophenyl)-4-(2-(4-(pyridin-3-yl)-1*H*-1,2,3-triazol-1-yl)ethyl)benzamide (24).** Compound **22** (316 mg, 1.03 mmol) and LiOH (74 mg, 3.09 mmol) in the mixed solvent THF/MeOH/H_2O (3:2:1, v/v, 12 mL) according to method described for the synthesis of compound **15g** gave compound **23** (272 mg, 90%) as a white solid. ^{1}H-NMR (DMSO-d6, 300 MHz) *δ*: 13.05 (s, 1H), 9.06 (s, 1H), 8.80 (s, 1H), 8.55-8.53 (m, 1H), 8.23 (d, *J* = 8.0 Hz, 1H), 7.96 (d, *J* = 8.4 Hz, 2H), 7.50-7.43 (m, 3H), 5.79 (s, 2H). ESI-MS (m/s): 295.35 [M+1].

To a stirred solution of **23** (261 mg, 0.89 mmol), Et_3N (136 μL, 0.98 mmol) and HBTU (372 mg, 0.98 mmol) in DMF (5 mL) was slowly added *o*-phenylenediamine (106 mg, 0.98 mmol) dropwise, and the mixture was stirred for 4 h at room temperature. Then, the mixture was diluted into water (40 mL) and extracted with EtOAc (40 mL × 3). The combined organic layers were dried over $MgSO_4$, concentrated and purified by silica gel column chromatography (CH_2Cl_2: MeOH =

100 : 2) to give compound **24** (92 mg, 27%) as a yellow solid. ^{1}H-NMR (DMSO-d_6, 300 MHz) δ: 9.59 (s, 1H), 9.01 (s, 1H), 8.70 (s, 1H), 8.52 (s, 1H), 8.17 (d, J = 6.9 Hz, 1H), 7.88 (d, J = 7.1 Hz, 2H), 7.46 (s, 1H), 7.35 (d, J = 7.2 Hz, 2H), 7.13 (d, J = 6.9 Hz, 1H), 6.99-6.91 (m, 1H), 6.76 (d, J = 7.4 Hz, 1H), 6.57 (t, J = 6.5 Hz, 1H), 4.86 (s, 2H), 4.74 (s, 2H). ^{13}C-NMR (DMSO-d_6, 150 MHz) δ: 165.49, 149.33, 146.80, 143.88, 143.63, 141.63, 133.46, 132.80, 129.09, 128.41, 127.20, 127.16, 126.92, 124.50, 123.79, 122.49, 116.69, 116.57, 50.90, 35.70. HRMS (ESI, negative) m/z calcd for $C_{22}H_{19}N_6O$ (M - H): 383.1626; found 383.1636.

1-(4-Ethynylphenyl)-3-(pyridin-3-ylmethyl)urea (27). A solution of 4-ethynyl-aniline (450 mg, 3.85 mmol) and CDI (750 mg, 4.62 mmol) in anhydrous THF (20 mL) was stirred at room temperature for 2 h. Then 3-(aminomethyl)pyridine (416 mg, 3.85 mmol) was added slowly, and the mixture was stirred at room temperature for another 12 h. The solution was evaporated in vacuo, and the residue was purified by column chromatography (CH_2Cl_2 : MeOH = 100 : 2) to give compound **27** (720 mg, 74%) as a yellow solid. ^{1}H-NMR (DMSO-d_6, 300 MHz) δ: 8.83 (s, 1H), 8.51 (d, J = 1.8 Hz, 1H), 8.44 (dd, J = 4.7, 1.5 Hz, 1H), 7.69 (d, J = 1.7 Hz, 1H), 7.44-7.29 (m, 5H), 6.77 (t, J = 5.9 Hz, 1H), 4.31 (d, J = 5.9 Hz, 2H), 3.98 (s, 1H). ESI-MS(m/s): 252.52 [M+1].

***N*-(2-Aminophenyl)-4-((4-(4-(3-(pyridin-3-ylmethyl)ureido)phenyl)-1*H*-1,2,3-triazol-1-yl)methyl)benzamide (30).** A solution of compound **27** (377 mg, 1.5 mmol), methyl 4-(azidomethyl)benzoate (287 mg, 1.5 mmol), VcNa (30 mg, 0.15 mmol) and $CuSO_4 \cdot 5H_2O$ (3.8 mg, 0.015 mmol) in the mixed solvent *t*-butanol/H_2O (1:1, v/v, 110

mL) was stirred at room temperature under N_2 protection condition for 12 h. The mixture was poured into water (30 mL), filtered and the precipitate was purified by column chromatography (Hexane : EtOAc = 1 : 2) to give compound **28** (456 mg, 69%) as a white powder. ^{1}H-NMR (DMSO-d_6, 300 MHz) δ: 8.73 (s, 1H), 8.49-8.47 (m, 3H), 7.96 (d, J = 8.2 Hz, 2H), 7.69 (d, J = 8.6 Hz, 2H), 7.44 (t, J = 8.8 Hz, 3H), 7.36 (s, 1H), 6.72 (d, J = 6.1 Hz, 1H), 5.72 (s, 2H), 4.31 (d, J = 5.8 Hz, 2H), 3.83 (s, 3H). ESI-MS (m/s): 443.28 [M+1].

Intermediate **28** (442 mg, 1.0 mmol) and LiOH (72 mg, 3.0 mmol) in the mixed solvent THF/MeOH/H_2O (3:2:1, v/v, 12 mL) according to method described for the synthesis of compound **15g** gave compound **29** (400 mg, 93%) as a white solid. ^{1}H-NMR (DMSO-d_6, 300 MHz) δ: 12.89 (s, 1H), 8.74 (s, 1H), 8.50-8.47 (m, 3H), 7.97 (d, J = 8.2 Hz, 2H), 7.0 (d, J = 8.6 Hz, 2H), 7.44 (t, J = 8.7 Hz, 3H), 7.37 (s, 1H), 6.72 (d, J = 6.2 Hz, 1H), 5.73 (s, 2H), 4.31 (d, J = 5.9 Hz, 2H). ESI-MS (m/s): 429.12 [M+1].

To a solution of compound **29** (381 mg, 0.89 mmol), Et_3N (136 μL, 0.98 mmol) and HBTU (372 mg, 0.98 mmol) in DMF (5 mL) was added *o*-phenylenediamine (106 mg, 0.98 mmol), and the mixture was stirred for 3 h at room temperature. Then, the mixture was diluted into water (40 mL) and extracted with EtOAc (40 mL × 3). The combined organic layers were dried over $MgSO_4$, concentrated and purified by silica gel column chromatography (CH_2Cl_2 : MeOH = 100 : 2) to give compound **30** (313 mg, 68%) as a yellow solid. ^{1}H-NMR (DMSO-d_6, 300 MHz) δ: 9.64 (s, 1H), 8.72 (s, 1H), 8.52 (s, 1H), 8.47-8.42 (m, 1H), 7.97 (d, J = 8.1 Hz, 2H), 7.74-7.66 (m, 3H),

7.50-7.40 (m, 4H), 7.35 (dd, J = 7.7, 4.8 Hz, 1H), 7.14 (d, J = 7.7 Hz, 1H), 6.95 (t, J = 7.5 Hz, 1H), 6.79-6.69 (m, 2H), 6.57 (t, J = 7.5 Hz, 1H), 5.70 (s, 2H), 4.88 (s, 2H), 4.32 (d, J = 5.7 Hz, 2H). ^{13}C-NMR (DMSO-d_6, 75 MHz) δ: 165.37, 155.64, 149.21, 148.50, 147.30, 143.61, 140.65, 139.71, 136.31, 135.46, 134.93, 128.74, 128.22, 127.16, 127.01, 126.17, 124.14, 123.93, 123.63, 121.14, 118.45, 116.68, 116.54, 53.08, 40.98. HRMS (ESI, negative) m/z calcd for $C_{29}H_{25}N_8O_2$ (M - H): 517.2106; found 517.2118.

4-Ethynyl-*N*-(pyridin-3-ylmethyl)benzamide (32). Compound **31** (292 mg, 2 mmol), Et_3N (218 μL, 2 mmol) and HBTU (758 mg, 2mmol) in DMF (5 mL) was slowly added 3-(aminomethyl)pyridine (216 mg, 2 mmol), and the mixture was stirred for 3 h at room temperature. Then the mixture was diluted by water (40 mL) and extracted with EtOAc (50 mL × 3). The organic layers were dried over $NaSO_4$, concentrated and purified by silica gel column chromatography (CH_2Cl_2 : MeOH = 100 : 3) to get compound **32** (212 mg, 45%) as a yellow solid. ^{1}H-NMR (DMSO-d_6, 300 MHz) δ: 9.20 (s, 1H), 8.55 (s, 1H), 8.47-8.45 (m, 1H), 7.89 (d, J = 8.3 Hz, 2H), 7.72 (d, J = 8.1 Hz, 1H), 7.58 (d, J = 8.5 Hz, 2H), 7.37 (dd, J = 4.8, 7.7 Hz, 1H), 4.51-4.40 (m, 3H). ESI-MS (m/s): 237.04 [M+1].

4-((4-(4-((pyridin-3-ylmethyl)carbamoyl)phenyl)-1*H*-1,2,3-triazol-1-yl)methyl)benzoate (33). A solution of compound **32** (354 mg, 1.5 mmol), methyl 4-(azidomethyl)benzoate (287 mg, 1.5 mmol), VcNa (30 mg, 0.15 mmol) and $CuSO_4 \cdot 5H_2O$ (3.8 mg, 0.015 mmol) in the mixed solvent *t*-butanol/H_2O (1:1, v/v, 110 mL) was stirred at room temperature under N_2 protection condition for 12 h. The

mixture was poured into water (30 mL), filtered and the precipitate was purified by column chromatography (Hexane : EtOAc = 1 : 2) to give compound **33** (286 mg, 67%) as a white powder. ^{1}H-NMR (DMSO-d_6, 300 MHz) δ: 9.18 (t, J = 5.8 Hz, 1H), 8.82 (s, 1H), 8.59 (s, 1H), 8.49 (d, J = 3.0 Hz, 1H), 8.06-7.97 (m, 6H), 7.78-7.75 (m, 1H), 7.51 (d, J = 8.1 Hz, 2H), 7.39 (dd, J = 7.8, 5.0 Hz, 1H), 5.79 (s, 2H), 4.53 (d, J = 5.7 Hz, 2H), 3.83 (s, 3H). ESI-MS (m/s): 428.19 [M+1].

4-((4-(4-((Pyridin-3-ylmethyl)carbamoyl)phenyl)-1*H*-1,2,3-triazol-1-yl)methyl)benzoic acid (34). Compound **27** (427 mg, 1.0 mmol) and LiOH (72 mg, 3.0 mmol) in the mixed solvent THF/MeOH/H_2O (3:2:1, v/v, 12 mL) according to method described for the synthesis of compound **15g** gave compound **34** (335 mg, 81%) as a white solid. ^{1}H-NMR (DMSO-d_6, 300 MHz) δ: 9.20 (t, J = 5.8 Hz, 1H), 8.83 (s, 1H), 8.60 (s, 1H), 8.49 (d, J = 3.0 Hz, 1H), 8.07-7.98 (m, 6H), 7.78-7.76 (m, 1H), 7.51 (d, J = 8.1 Hz, 2H), 7.39 (dd, J = 7.8, 5.0 Hz, 1H), 5.80 (s, 2H), 4.54 (d, J = 5.7 Hz, 2H). ESI-MS (m/s): 414.16 [M+1].

***N*-(2-Aminophenyl)-4-((4-(4-((pyridin-3-ylmethyl)carbamoyl)phenyl)-1*H*-1,2,3-triazol-1-yl)methyl)benzamide (35).** To a solution of compound **34** (100 mg, 0.24 mmol), Et_3N (36 μL, 0.26 mmol) and HBTU (98 mg, 0.26 mmol) in DMF (5 mL) was added *o*-phenylenediamine (28 mg, 0.26 mmol), and the mixture was stirred for 3 h at room temperature. Then, the mixture was diluted into water (40 mL) and extracted with EtOAc (40 mL × 3). The combined organic layers were dried over $MgSO_4$, concentrated and purified by silica gel column chromatography (CH_2Cl_2 : MeOH = 100 : 2) to give compound **35** (60 mg, 50%) as a yellow solid. ^{1}H-NMR (DMSO-d_6,

300 MHz) δ: 9.71 (s, 1H), 9.18 (t, J = 5.8 Hz, 1H), 8.82 (s, 1H), 8.59 (s, 1H), 8.49 (d, J = 3.0 Hz, 1H), 8.06-7.97 (m, 6H), 7.78-7.75 (m, 1H), 7.51 (d, J = 8.1 Hz, 2H), 7.39 (dd, J = 7.8, 5.0 Hz, 1H), 7.17 (d, J = 7.8 Hz, 1H), 7.02-6.96 (m, 1H), 6.81-6.78 (m, 1H), 6.61 (t, J = 7.8 Hz, 1H), 5.79 (s, 2H), 4.98 (s, 2H), 4.53 (d, J = 5.7 Hz, 2H). ^{13}C-NMR (DMSO-d_6, 75 MHz) δ: 166.34, 165.33, 149.29, 148.51, 146.41, 143.58, 139.47, 135.68, 135.58, 134.97, 133.82, 133.71, 128.77, 128.45, 128.30, 127.17, 127.02, 125.41, 123.97, 123.60, 122.99, 116.69, 116.54, 53.21. HRMS (ESI, negative) m/z calcd for $C_{29}H_{24}N_7O_2$ (M - H): 502.1997; found 502.2000.

***In vitro* NAMPT Inhibition Assay.** NAMPT inhibitory activity of the target compounds was measured using a fluorometric method as previously described.[22] The reaction mixture contained 50 mM Tris-HCl (pH 7.5), 0.02 % BSA, 12 mM $MgCl_2$, 2 mM ATP, 0.4 mM PRPP, 2 mM DTT, 2 μg/mL NAMPT, the compound with various concentrations (1% DMSO), in a final volume of 25 μL. The reaction mixture was incubated at 37 ^{o}C for 5 min and then 4.5 μL NAM was added to initiate the enzyme reaction, resulting in a final concentration of 0.2 μM NAM. After reacting at 37 ^{o}C for 15 min, the enzyme reaction was terminated by heating at 95 ^{o}C for 1 min and cooling in an ice bath. After that, the mixture was added 10 μL 20% acetophenone in DMSO and 10 μL 2 M KOH and then was vortex-mixed and kept in ice bath for 2 min. Finally, 45 μL 88% formic acid was added, which was incubated at 37 ^{o}C for another 10 min. Fluorescence was then analyzed with an excitation of 382 nm and an emission wavelength of 445 nm at Spectra Max M5 microtiter plate reader. The IC_{50} values were calculated using nonlinear regression with normalized dose-response fit

using Prism GraphPad software.

***In vitro* HDAC Inhibition Assay.** The HDAC1 (#AB101661) and HDAC6 (#AB42632) enzymes were purchased from Abcam. HDAC3 (#BML-SE515-0050) was purchased from ENZO Inc. HDAC4 (#H86-31G) and HDAC8 (#H90-30H) was purchased from SignalChem. The reaction mixture contained 25 mM Tris (pH 8.0), 1 mM $MgCl_2$, 0.1 mg/ml BSA, 137mM NaCl, 2.7 mM KCl, HDAC (HDAC1, 7.2 ng/well; HDAC2, 7.5 ng/well; HDAC3, 3.4 ng/well; HDAC4, 0.3 ng/well; HDAC6, 15 ng/well; HDAC8, 22 ng/well) in a total volume of 40 μL. The test compounds (3-fold dilution, 10 concentrations) were diluted in 10% DMSO and 5 μL of the dilution was added and preincubated with purified recombinant HDAC at room temperature for 5 min before substrate addition. Finaly, the enzyme substrate (Ac-Leu-Gly-Lys(Ac)-AMC, 10 μM for HDAC1, 2, 3, 6; Ac-Leu-Gly-Lys(Tfa)-AMC, 2 μM for HDAC4 and HDAC8) was added and the plate was incubated at 37 ℃ for 30 min in a final volume of 50 μL. The reaction was quenched with 50 μL HDAC assay developer (1 mg/mL trypsin and 2 μM TSA in assay buffer) for 30 min at room temperature. The assay was performed by quantitating the fluorescent product amount of in solution following an enzyme reaction. Fluorescence was then analyzed with an excitation of 350-360 nm and an emission wavelength of 450-460 nm at Spectra Max M5 microtiter plate reader. The IC_{50} values were calculated using nonlinear regression with normalized dose-response fit using Prism GraphPad software. All experiments were independently performed at least three times.

***In vitro* Cytotoxicity Assay.** Three human cancer cell lines, HCT116, MDA-MB-231

and HepG2, which were in the logarithmic phase, were harvested and plated in 96-well microtiter plates at a density of 5×10^3/well and incubated in a humidified atmosphere with 5% CO_2 at 37 ^oC for 24 h. The cells were exposed to different concentrations (three-times step dilution) of the test compounds for 72 h in three replicates and 0.1% DMSO for control. After that, 20 μL of MTT (3-(4,5-dimethylthiazol-2-yl)-2,5-diphenyltetrazoliumbromide) solution (5 mg/mL) was added and the plate was incubated for another 4 h. The formazan was dissolved in 100 μL of DMSO. The absorbance (OD) was then read on a WellscanMK-2 microplate reader (Labsystems) at 570 nm. The concentration causing 50% inhibition of cell growth (IC_{50}) was determined by the Logit method.[49] All experiments were performed three times.

***In vivo* Antitumor Activity.** The experimental procedures and the animal use and care protocols were approved by the Committee on Ethical Use of Animals of Second military medical university. BALB/C nude male mice (Certificate SCXK-2007-0005, weighing 18 g to 20 g) were obtained from Shanghai Experimental Animal Center, Chinese Academy of Sciences. HCT116 colon cancer cell suspensions were implanted subcutaneously into the right axilla region of mice. Treatment was begun when implanted tumors had reached a volume of about 100-300 mm^3. The animals were randomized into appropriate groups (five animals/treatment and eight animals for the control group). For the test of compound **6**, control mice received vehicle (0.5% carboxymethyl cellulose). Compound **6** was suspended in the 0.5% carboxymethyl cellulose and administered po at the dose of 25 mg/kg/day for 14

consecutive days. For the test of compound **1**, **2** and **35**, compounds were dissolved in 0.1% Tween 80 in normal saline. All mice were administered by ip injection with compounds or vehicle as control twice a day for 21 consecutive days. Tumor volumes were monitored by caliper measurement of the length and width and calculated using the formula of $TV = 1/2\times a \times b^2$, where a is the tumor length and b is the width. Tumor volumes and body weights were monitored every 3 days over the course of treatment. Mice were sacrificed on day 30 to 33 after implantation of cells and tumors were removed and recorded for analysis.

NAD Measurement. Cellular level of NAD was measured by spectrophotometric enzymatic cycling assay, as described previously[50-52]. Briefly, cells were seeded in 96-well plate and starved for over 12 h with serum-free DMEM at 60~70% confluency, following by treatment with compounds or vehicle for 24 h. Cells were lysed with 50 μL of 1 M $HClO_4$ on ice for 30 min. The lysates were cleared by centrifuging at 4 °C at 18000 × g for 5 min, and cleared lysates (40 μL) were neutralized by adding 1 M K_2CO_3 (16 μL) and incubated on ice for 20 min. After centrifuging for 10 min, 10 μL of supernatant were mixed with reaction buffer [50 mM Tris-HCl (pH 7.5), 3% ethanol, 1.66 mM PES (phenazineethosulfate), 0.42 mM MTT (3-(4,5-dimethylthiazolyl-2)-2,5-diphenyltetrazolium bromide), 90 μg/mL ADH (alcohol dehydrogenase)] in a total volume of 100 μL, and incubated at 37 °C for 40 min. The absorbance at 570 nm was determined. A blank measurement without ADH was also carried out. Each experiment was carried out in triplicate in three replicate wells.

Cellular Thermal Shift Assay (CETSA). CESTA was performed as previously described.[53] In the intact cell experiments, treated cells were exposed to a drug for 3 h in cell culture incubator (95% O_2 and 5% CO_2). Control cells were incubated with an equal volume of diluent for the corresponding drug. Compound **35** was added from DMSO stocks to the final concentration of 10 μM and DMSO concentration 0.1% except those in $ITDRF_{CESTA}$. Following the incubation, the cells were harvested using Trypsin/EDTA solution and washed with PBS in order to remove excess drug. Equal amounts of cell suspensions were aliquoted into 0.2 mL PCR microtubes, and excess PBS was removed by centrifugation to leave 10 μL or less PBS in each microtube. The cell suspensions were freeze-thawed three times using liquid nitrogen. The soluble fraction (lysate) was separated from the cell debris by centrifugation at 20000 × g for 20 min at 4°C. The cell lysates were diluted with PBS. The respective lysates were divided into smaller (50 μL) aliquots and heated individually at different temperatures for 3 min (Veriti thermal cycler, Applied Biosystems/Life Technologies) followed by cooling for 3 min at room temperature. The heated lysates were centrifuged at 20000 × g for 20 min at 4°C in order to separate the soluble fractions from precipitates. The supernatants were transferred to new microtubes and analyzed by sodium dodecyl sulfate polyacrylamide gel electrophoresis (SDS-PAGE) followed by Western blot analysis. Target proteins in CESTA were examined by SDS-PAGE and immunoblotting as previously described.[52-55] The primary antibodies for Western blotting were specific for the following: NAMPT (Santa Cruz, sc-67020, used at 1:500)。

Western Blot of Histone Hyperacetylation and Autophagy Detection. In histone hyperacetylation assay, human HCT116 cells were exposed to compound **35** at 1 and 5 μM for 24 h and then harvested and washed with PBS three times. Then the cells were lysed with RIPA Cell Lysis Buffer on ice for 30 min. The cell lysates were centrifuged at 12000 × g for 15 min at 4 ^{o}C. Supernatant was collected and BCA Protein Assay was used for determined protein concentration. Equal amounts of protein (30 μg) was separated by SDS-PAGE. Then the proteins were transferred to polyvinylidene fluoride membranes and were blocked with 5% BSA for 2 h. The membranes were incubated with the primary antibody overnight at 4 °C and were washed with TBST for three times. Then the mixture was incubated with the secondary antibody for 1.5 h. The membranes were washed with TBST for three times. The immunoblots were visualized by Odyssey Infrared Imaging.

In autophagy detection assay, human HCT116 cells were exposed to compound **35** at 5 μM for 24-72 h. Then the assay was performed as described above. The antibodies including anti-Histone H3 (#ab1791, Abcam), anti-Histone H4 (#ab9051, Abcam), anti-Nampt (#ab45890, Abcam), anti-P62 (#ab56416, Abcam), anti-LC3II (#ab48394, Abcam) were purchased from Abcam.

Flow Cytometer Analysis of Cell Cycle. HCT116 cells (2×10^4 cells/mL) were treated with compound **35** at 1 and 5 μM for 48 h. The treated cells were collected, resuspended, and incubated for 30 min at 37°C with 25 μg/mL PI and 10 μg/mL RNase buffer. For each sample, at least 1×10^4 cells were analyzed using flow cytometry (BD Accuri C6).

Apoptosis Detection Assay. HCT116 cells (5×10^5 cells/mL) were seeded in six-well plates and treated with compounds at concentration of 5 μM for 72 h. For the assay to illustrate autophagic function of **35**, HCT116 cells were incubated with autophagy inhibitor wortmannin for 1 h and subsequently treated with **35** for 72 h. The cells were then harvested by trypsinization and washed twice with cold PBS. After centrifugation and removal of the supernatants, cells were resuspended in 400 μL of 1 × binding buffer which was then added to 5 μL of annexin V-FITC and incubated at room temperature for 15 min. After adding 10 μL of PI the cells were incubated at room temperature for another 15 min in dark. The stained cells were analyzed by a Flow Cytometer (BD Accuri C6).

Molecular docking. The crystal structure of NAMPT in complex with **2** was obtained from protein database bank (PDB ID: 2GVJ)[56] and prepared for docking using the protein preparation tool in Discovery Studio 3.0.[40] During this process, the ligands and waters were removed and hydrogens were added to the structure. Staged minimization was performed with default setting. The docking studies were carried out using GOLD 5.0.[57] Binding site was defined as whole residues within a 10 Å radius subset encompassing the **2**. Conformations were generated by genetic algorithm and scored using GoldScore as fitness function. The best conformation was chosen to analyse the ligand–protein interaction. The image representing the best pose was prepared using PyMOL. Docking analysis was performed on HDAC1 (PDB ID: 4BKX)[58, 59] as described above.

■ ASSOCIATED CONTENT

Supporting Information

Figure of NAD biosynthetic pathways, results of molecular dynamics simulations, synergistic effects of **2** and **5** *in vitro*, mean plasma concentration-time profiles and pharmacokinetic parameters of **1**, **2** and **35**, synthetic methods and characterization data for compound **6**, methods for pharmacokinetic studies and molecular dynamics simulations, ^{1}HNMR and HRMS spectra of the representative compounds, and Molecular Formula Strings of the target compounds.

The Supporting Information is available free of charge on the ACS Publications website at DOI: XXXXXX/acs.jmedchem.XXXXXXX.

■ AUTHOR INFORMATION

Corresponding Author

* (C. S.) Phone / Fax: +86 21 81871239. E-mail: shengcq@smmu.edu.cn

* (C. M.) Phone / Fax: +86 21 81871239. E-mail: cymiao@smmu.edu.cn.

* (Y. R.) Phone / Fax: +86 10 62782025. E-mail: yrao@tsinghua.edu.cn

Author Contributions

† Guoqiang Dong, Wei Chen, Xia Wang, contributed equally to this work.

The manuscript was written through contributions of all authors. All authors have given approval to the final version of the manuscript.

Notes

The authors declare no competing financial interest.

■ ACKNOWLEDGMENT

This work was supported by the National Natural Science Foundation of China (Grant 81402796, 81222044), Science and Technology Commission of Shanghai

Municipality (Grant 14YF1405400), and Shanghai Education Development Foundation and Shanghai Municipal Education Commission (Chenguang Program, Grant 15CG42).

■ ABBREVIATIONS LIST

NAMPT, nicotinamide phosphoribosyltransferase; HDAC, histone deacetylase; HDACi, HDAC inhibitor; NAD, nicotinamide adenine dinucleotide; Trp, tryptophan; NAM, nicotinamide; AMC, 7-amino-4-methylcoumarin; ZBG, zinc-binding group; PK, pharmacokinetic; CETSA, cellular thermal shift assay; TCDI, 1,1'-thiocarbonyldiimidazole; CDI, *N*,*N*'-Carbonyldiimidazole; HBTU, *O*-Benzotriazole-*N*,*N*,*N*,*N*-tetramethyl-uronium-hexafluorophosphate; TGI, tumor growth inhibition; ADH, alcohol dehydrogenase. VcNa, sodium ascorbate.

■ REFERENCES

1. Peters, J. U. Polypharmacology - foe or friend? *J. Med. Chem.* **2013**, *56*, 8955-8971.

2. Anighoro, A.; Bajorath, J.; Rastelli, G. Polypharmacology: challenges and opportunities in drug discovery. *J. Med. Chem.* **2014**, *57*, 7874-7887.

3. Zimmermann, G. R.; Lehar, J.; Keith, C. T. Multi-target therapeutics: when the whole is greater than the sum of the parts. *Drug Discovery Today* **2007**, *12*, 34-42.

4. Ciceri, P.; Muller, S.; O'Mahony, A.; Fedorov, O.; Filippakopoulos, P.; Hunt, J. P.; Lasater, E. A.; Pallares, G.; Picaud, S.; Wells, C.; Martin, S.; Wodicka, L. M.; Shah, N. P.; Treiber, D. K.; Knapp, S. Dual kinase-bromodomain inhibitors for rationally

designed polypharmacology. *Nat. Chem. Biol.* **2014**, *10*, 305-312.

5. Haber, D. A.; Gray, N. S.; Baselga, J. The evolving war on cancer. *Cell* **2011**, *145*, 19-24.

6. Trusolino, L.; Bertotti, A. Compensatory pathways in oncogenic kinase signaling and resistance to targeted therapies: six degrees of separation. *Cancer Discovery* **2012**, *2*, 876-880.

7. Morphy, R.; Rankovic, Z. Designed multiple ligands. An emerging drug discovery paradigm. *J. Med. Chem.* **2005**, *48*, 6523-6543.

8. Besnard, J.; Ruda, G. F.; Setola, V.; Abecassis, K.; Rodriguiz, R. M.; Huang, X. P.; Norval, S.; Sassano, M. F.; Shin, A. I.; Webster, L. A.; Simeons, F. R.; Stojanovski, L.; Prat, A.; Seidah, N. G.; Constam, D. B.; Bickerton, G. R.; Read, K. D.; Wetsel, W. C.; Gilbert, I. H.; Roth, B. L.; Hopkins, A. L. Automated design of ligands to polypharmacological profiles. *Nature* **2012**, *492*, 215-220.

9. Conway, S. J.; Woster, P. M.; Shen, J. K.; Georg, G.; Wang, S. Epigenetics: novel therapeutics targeting epigenetics. *J. Med. Chem.* **2015**, *58*, 523-524.

10. Ververis, K.; Hiong, A.; Karagiannis, T. C.; Licciardi, P. V. Histone deacetylase inhibitors (HDACIs): multitargeted anticancer agents. *Biol.: Targets Ther.* **2013**, *7*, 47-60.

11. Mann, B. S.; Johnson, J. R.; Cohen, M. H.; Justice, R.; Pazdur, R. FDA approval summary: vorinostat for treatment of advanced primary cutaneous T-cell lymphoma. *Oncologist* **2007**, *12*, 1247-1252.

12. Bailey, H.; Stenehjem, D. D.; Sharma, S. Panobinostat for the treatment of

multiple myeloma: the evidence to date. *J. Blood Med.* **2015**, *6*, 269-276.

13. Manal, M.; Chandrasekar, M. J.; Gomathi Priya, J.; Nanjan, M. J. Inhibitors of histone deacetylase as antitumor agents: a critical review. *Bioorg. Chem.* **2016**, *67*, 18-42.

14. Lai, C. J.; Bao, R.; Tao, X.; Wang, J.; Atoyan, R.; Qu, H.; Wang, D. G.; Yin, L.; Samson, M.; Forrester, J.; Zifcak, B.; Xu, G. X.; DellaRocca, S.; Zhai, H. X.; Cai, X.; Munger, W. E.; Keegan, M.; Pepicelli, C. V.; Qian, C. CUDC-101, a multitargeted inhibitor of histone deacetylase, epidermal growth factor receptor, and human epidermal growth factor receptor 2, exerts potent anticancer activity. *Cancer. Res.* **2010**, *70*, 3647-3656.

15. Papavassiliou, K. A.; Papavassiliou, A. G. Histone deacetylases inhibitors: conjugation to other anti-tumour pharmacophores provides novel tools for cancer treatment. *Expert Opin. Invest. Drugs* **2014**, *23*, 291-294.

16. Yuneva, M. O.; Fan, T. W.; Allen, T. D.; Higashi, R. M.; Ferraris, D. V.; Tsukamoto, T.; Mates, J. M.; Alonso, F. J.; Wang, C.; Seo, Y.; Chen, X.; Bishop, J. M. The metabolic profile of tumors depends on both the responsible genetic lesion and tissue type. *Cell Metab.* **2012**, *15*, 157-170.

17. Galli, U.; Travelli, C.; Massarotti, A.; Fakhfouri, G.; Rahimian, R.; Tron, G. C.; Genazzani, A. A. Medicinal chemistry of nicotinamide phosphoribosyltransferase (NAMPT) inhibitors. *J. Med. Chem.* **2013**, *56*, 6279-6296.

18. Sotgia, F.; Martinez-Outschoorn, U. E.; Lisanti, M. P. Cancer metabolism: new validated targets for drug discovery. *Oncotarget* **2013**, *4*, 1309-1316.

19. Galluzzi, L.; Kepp, O.; Vander Heiden, M. G.; Kroemer, G. Metabolic targets for cancer therapy. *Nat. Rev. Drug Discovery* **2013**, *12*, 829-846.

20. Sampath, D.; Zabka, T. S.; Misner, D. L.; O'Brien, T.; Dragovich, P. S. Inhibition of nicotinamide phosphoribosyltransferase (NAMPT) as a therapeutic strategy in cancer. *Pharmacol. Ther.* **2015**, *151*, 16-31.

21. Bai, J.; Liao, C.; Liu, Y.; Qin, X.; Chen, J.; Qiu, Y.; Qin, D.; Li, Z.; Tu, Z. C.; Jiang, S. Structure-based design of potent nicotinamide phosphoribosyltransferase inhibitors with promising in vitro and in vivo antitumor activities. *J. Med. Chem.* **2016**, *59*, 5766-5779.

22. Xu, T. Y.; Zhang, S. L.; Dong, G. Q.; Liu, X. Z.; Wang, X.; Lv, X. Q.; Qian, Q. J.; Zhang, R. Y.; Sheng, C. Q.; Miao, C. Y. Discovery and characterization of novel small-molecule inhibitors targeting nicotinamide phosphoribosyltransferase. *Sci. Rep.* **2015**, *5*, 10043.

23. Beauparlant, P.; Bedard, D.; Bernier, C.; Chan, H.; Gilbert, K.; Goulet, D.; Gratton, M. O.; Lavoie, M.; Roulston, A.; Turcotte, E.; Watson, M. Preclinical development of the nicotinamide phosphoribosyl transferase inhibitor prodrug GMX1777. *Anticancer Drugs* **2009**, *20*, 346-354.

24. Watson, M.; Roulston, A.; Belec, L.; Billot, X.; Marcellus, R.; Bedard, D.; Bernier, C.; Branchaud, S.; Chan, H.; Dairi, K.; Gilbert, K.; Goulet, D.; Gratton, M. O.; Isakau, H.; Jang, A.; Khadir, A.; Koch, E.; Lavoie, M.; Lawless, M.; Nguyen, M.; Paquette, D.; Turcotte, E.; Berger, A.; Mitchell, M.; Shore, G. C.; Beauparlant, P. The small molecule GMX1778 is a potent inhibitor of NAD+ biosynthesis: strategy for

enhanced therapy in nicotinic acid phosphoribosyltransferase 1-deficient tumors. *Mol. Cell. Biol.* **2009**, *29*, 5872-5888.

25. Hasmann, M.; Schemainda, I. FK866, a highly specific noncompetitive inhibitor of nicotinamide phosphoribosyltransferase, represents a novel mechanism for induction of tumor cell apoptosis. *Cancer Res.* **2003**, *63*, 7436-7442.

26. Holen, K.; Saltz, L. B.; Hollywood, E.; Burk, K.; Hanauske, A. R. The pharmacokinetics, toxicities, and biologic effects of FK866, a nicotinamide adenine dinucleotide biosynthesis inhibitor. *Invest. New Drugs* **2008**, *26*, 45-51.

27. von Heideman, A.; Berglund, A.; Larsson, R.; Nygren, P. Safety and efficacy of NAD depleting cancer drugs: results of a phase I clinical trial of CHS 828 and overview of published data. *Cancer Chemother. Pharmacol.* **2010**, *65*, 1165-1172.

28. Cea, M.; Soncini, D.; Fruscione, F.; Raffaghello, L.; Garuti, A.; Emionite, L.; Moran, E.; Magnone, M.; Zoppoli, G.; Reverberi, D.; Caffa, I.; Salis, A.; Cagnetta, A.; Bergamaschi, M.; Casciaro, S.; Pierri, I.; Damonte, G.; Ansaldi, F.; Gobbi, M.; Pistoia, V.; Ballestrero, A.; Patrone, F.; Bruzzone, S.; Nencioni, A. Synergistic interactions between HDAC and sirtuin inhibitors in human leukemia cells. *PLoS One* **2011**, *6*, e22739.

29. Bartucci, M. A.; Ciszek, J. W. Substituent parameters impacting isomer composition and optical properties of dihydroindolizine molecular switches. *J. Org. Chem.* **2014**, *79*, 5586-5594.

30. Rostovtsev, V. V.; Green, L. G.; Fokin, V. V.; Sharpless, K. B. A stepwise huisgen cycloaddition process: copper(I)-catalyzed regioselective "ligation" of azides and

terminal alkynes. *Angew. Chem. Int. Ed. Engl.* **2002**, *41*, 2596-2599.

31. Wang, X.; Xu, T. Y.; Liu, X. Z.; Zhang, S. L.; Wang, P.; Li, Z. Y.; Guan, Y. F.; Wang, S. N.; Dong, G. Q.; Zhuo, S.; Le, Y. Y.; Sheng, C. Q.; Miao, C. Y. Discovery of novel inhibitors and fluorescent probe targeting NAMPT. *Sci. Rep.* **2015**, *5*, 12657.

32. Chen, W.; Dong, G.; He, S.; Xu, T.; Wang, X.; Liu, N.; Zhang, W.; Miao, C.; Sheng, C. Identification of benzothiophene amides as potent inhibitors of human nicotinamide phosphoribosyltransferase. *Bioorg. Med. Chem. Lett.* **2016**, *26*, 765-768.

33. Zheng, X.; Bauer, P.; Baumeister, T.; Buckmelter, A. J.; Caligiuri, M.; Clodfelter, K. H.; Han, B.; Ho, Y. C.; Kley, N.; Lin, J.; Reynolds, D. J.; Sharma, G.; Smith, C. C.; Wang, Z.; Dragovich, P. S.; Oh, A.; Wang, W.; Zak, M.; Gunzner-Toste, J.; Zhao, G.; Yuen, P. W.; Bair, K. W. Structure-based identification of ureas as novel nicotinamide phosphoribosyltransferase (Nampt) inhibitors. *J. Med. Chem.* **2013**, *56*, 4921-4937.

34. Gryder, B. E.; Sodji, Q. H.; Oyelere, A. K. Targeted cancer therapy: giving histone deacetylase inhibitors all they need to succeed. *Future Med. Chem.* **2012**, *4*, 505-524.

35. Moradei, O. M.; Mallais, T. C.; Frechette, S.; Paquin, I.; Tessier, P. E.; Leit, S. M.; Fournel, M.; Bonfils, C.; Trachy-Bourget, M. C.; Liu, J.; Yan, T. P.; Lu, A. H.; Rahil, J.; Wang, J.; Lefebvre, S.; Li, Z.; Vaisburg, A. F.; Besterman, J. M. Novel aminophenyl benzamide-type histone deacetylase inhibitors with enhanced potency and selectivity. *J. Med. Chem.* **2007**, *50*, 5543-5546.

36. Li, X.; Inks, E. S.; Hou, J.; Chou, C. J.; Zhang, J.; Jiang, Y.; Zhang, Y.; Xu, W. Discovery of the first N-hydroxycinnamamide-based histone deacetylase 1/3 dual

inhibitors with potent oral antitumor activity. *J. Med. Chem.* **2014**, *57*, 3324-3341.

37. Shaw, D. E. A fast, scalable method for the parallel evaluation of distance-limited pairwise particle interactions. *J. Comput. Chem.* **2005**, *26*, 1318-1328.

38. Wagner, F. F.; Lundh, M.; Kaya, T.; McCarren, P.; Zhang, Y. L.; Chattopadhyay, S.; Gale, J. P.; Galbo, T.; Fisher, S. L.; Meier, B. C.; Vetere, A.; Richardson, S.; Morgan, N. G.; Christensen, D. P.; Gilbert, T. J.; Hooker, J. M.; Leroy, M.; Walpita, D.; Mandrup-Poulsen, T.; Wagner, B. K.; Holson, E. B. An isochemogenic set of inhibitors to define the therapeutic potential of histone deacetylases in beta-cell protection. *ACS Chem. Biol.* **2016**, *11*, 363-374.

39. He, S.; Dong, G.; Wang, Z.; Chen, W.; Huang, Y.; Li, Z.; Jiang, Y.; Liu, N.; Yao, J.; Miao, Z.; Zhang, W.; Sheng, C. Discovery of novel multiacting topoisomerase I/II and histone deacetylase inhibitors. *ACS Med. Chem. Lett.* **2015**, *6*, 239-243.

40. Colombano, G.; Travelli, C.; Galli, U.; Caldarelli, A.; Chini, M. G.; Canonico, P. L.; Sorba, G.; Bifulco, G.; Tron, G. C.; Genazzani, A. A. A novel potent nicotinamide phosphoribosyltransferase inhibitor synthesized via click chemistry. *J. Med. Chem.* **2010**, *53*, 616-623.

41. Nahimana, A.; Attinger, A.; Aubry, D.; Greaney, P.; Ireson, C.; Thougaard, A. V.; Tjornelund, J.; Dawson, K. M.; Dupuis, M.; Duchosal, M. A. The NAD biosynthesis inhibitor APO866 has potent antitumor activity against hematologic malignancies. *Blood* **2009**, *113*, 3276-3286.

42. Billington, R. A.; Genazzani, A. A.; Travelli, C.; Condorelli, F. NAD depletion by FK866 induces autophagy. *Autophagy* **2008**, *4*, 385-387.

43. Shao, Y.; Gao, Z.; Marks, P. A.; Jiang, X. Apoptotic and autophagic cell death induced by histone deacetylase inhibitors. *Proc. Natl. Acad. Sci. U. S. A.* **2004**, *101*, 18030-18035.

44. Chiao, M. T.; Cheng, W. Y.; Yang, Y. C.; Shen, C. C.; Ko, J. L. Suberoylanilide hydroxamic acid (SAHA) causes tumor growth slowdown and triggers autophagy in glioblastoma stem cells. *Autophagy* **2013**, *9*, 1509-1526.

45. Wang, S.; Fang, K.; Dong, G.; Chen, S.; Liu, N.; Miao, Z.; Yao, J.; Li, J.; Zhang, W.; Sheng, C. Scaffold diversity inspired by the natural product evodiamine: discovery of highly potent and multitargeting antitumor agents. *J. Med. Chem.* **2015**, *58*, 6678-6696.

46. Dong, G.; Wang, S.; Miao, Z.; Yao, J.; Zhang, Y.; Guo, Z.; Zhang, W.; Sheng, C. New tricks for an old natural product: discovery of highly potent evodiamine derivatives as novel antitumor agents by systemic structure-activity relationship analysis and biological evaluations. *J. Med. Chem.* **2012**, *55*, 7593-7613.

47. Subramanian, S.; Bates, S. E.; Wright, J. J.; Espinoza-Delgado, I.; Piekarz, R. L. Clinical toxicities of histone deacetylase inhibitors. *Pharmaceuticals* **2010**, *3*, 2751-2767.

48. Gao, Y.; Zou, X.-M.; Yu, L.-M.; Xu, H.; Liu, B.; Zhu, Y.-Q.; Hu, F.-Z.; Yang, H.-Z. Synthesis and herbicidal activity of 2-cyano-3-methylthio-3-substituted methylaminoacrylates. *Chin. J. Chem* . **2006**, *24*, 521-526.

49. Dong, G.; Sheng, C.; Wang, S.; Miao, Z.; Yao, J.; Zhang, W. Selection of evodiamine as a novel topoisomerase I inhibitor by structure-based virtual screening

and hit optimization of evodiamine derivatives as antitumor agents. *J. Med. Chem.* **2010**, *53*, 7521-7531.

50. Matsumura, H.; Miyachi, S. Cycling assay for nicotinamide adenine dinucleotides. *Methods Enzymol.* **1980**, *69*, 465-470.

51. Wang, P.; Zhang, R. Y.; Song, J.; Guan, Y. F.; Xu, T. Y.; Du, H.; Viollet, B.; Miao, C. Y. Loss of AMP-activated protein kinase-alpha2 impairs the insulin-sensitizing effect of calorie restriction in skeletal muscle. *Diabetes* **2012**, *61*, 1051-1061.

52. Wang, P.; Xu, T. Y.; Guan, Y. F.; Tian, W. W.; Viollet, B.; Rui, Y. C.; Zhai, Q. W.; Su, D. F.; Miao, C. Y. Nicotinamide phosphoribosyltransferase protects against ischemic stroke through SIRT1-dependent adenosine monophosphate-activated kinase pathway. *Ann. Neurol.* **2011**, *69*, 360-374.

53. Martinez Molina, D.; Jafari, R.; Ignatushchenko, M.; Seki, T.; Larsson, E. A.; Dan, C.; Sreekumar, L.; Cao, Y.; Nordlund, P. Monitoring drug target engagement in cells and tissues using the cellular thermal shift assay. *Science* **2013**, *341*, 84-87.

54. Xu, T. Y.; Guo, L. L.; Wang, P.; Song, J.; Le, Y. Y.; Viollet, B.; Miao, C. Y. Chronic exposure to nicotine enhances insulin sensitivity through alpha7 nicotinic acetylcholine receptor-STAT3 pathway. *PLoS One* **2012**, *7*, e51217.

55. Wang, P.; Xu, T. Y.; Guan, Y. F.; Zhao, Y.; Li, Z. Y.; Lan, X. H.; Wang, X.; Yang, P. Y.; Kang, Z. M.; Vanhoutte, P. M.; Miao, C. Y. Vascular smooth muscle cell apoptosis is an early trigger for hypothyroid atherosclerosis. *Cardiovasc. Res.* **2014**, *102*, 488-459.

56. Khan, J. A.; Tao, X.; Tong, L. Molecular basis for the inhibition of human

NMPRTase, a novel target for anticancer agents. *Nat. Struct. Mol. Biol.* **2006**, *13*, 582-588.

57. Jones, G.; Willett, P.; Glen, R. C.; Leach, A. R.; Taylor, R. Development and validation of a genetic algorithm for flexible docking. *J. Mol. Biol.* **1997**, *267*, 727-748.

58. Millard, C. J.; Watson, P. J.; Celardo, I.; Gordiyenko, Y.; Cowley, S. M.; Robinson, C. V.; Fairall, L.; Schwabe, J. W. Class I HDACs share a common mechanism of regulation by inositol phosphates. *Mol. Cell* **2013**, *51*, 57-67.

59. Hassanzadeh, M.; Bagherzadeh, K.; Amanlou, M. A comparative study based on docking and molecular dynamics simulations over HDAC-tubulin dual inhibitors. *J. Mol. Graphics Modell.* **2016**, *70*, 170-180.

Table of Contents Graphic